Remote Sensing of Environment 211 (2018) 276–291

Contents lists available at ScienceDirect

Remote Sensing of Environment

journal homepage: www.elsevier.com/locate/rse

Retrieving structural and chemical properties of individual tree crowns in a highly diverse tropical forest with 3D radiative transfer modeling and imaging spectroscopy

Matheus Pinheiro Ferreira[a,*], Jean-Baptiste Féret[b], Eloi Grau[b], Jean-Philippe Gastellu-Etchegorry[c], Cibele Hummel do Amaral[e], Yosio Edemir Shimabukuro[a], Carlos Roberto de Souza Filho[d]

[a] Remote Sensing Division, National Institute for Space Research, Av. dos Astronautas 1758, 12227-010, São José dos Campos, SP, Brazil
[b] TETIS, Irstea, AgroParisTech, CIRAD, CNRS, Université Montpellier, Montpellier, France, Maison de la Télédétection, 500 Rue Jean-François Breton, 34000, Montpellier, France
[c] Centre d'Etudes Spatiales de la BIOsphère (CESBIO) - UPS, CNES, CNRS, IRD, Université de Toulouse, 31401 Toulouse Cedex 9, France
[d] Geosciences Institute, University of Campinas, R. João Pandiá Calógeras 51, 13083-870, Campinas, SP, Brazil
[e] Departamento de Engenharia Florestal, Avenida Peter Henry Rolfs, s/n - Campus Universitário, Viçosa 36570-900, Brazil

ARTICLE INFO

Keywords:
Hyperspectral remote sensing
DART
Functional traits
Model inversion
Tree species classification
Tropical forest

ABSTRACT

Spatial and temporal information on the structural and chemical properties of tropical forest canopies are key to understanding ecosystem processes. However, such information is usually limited to field studies performed at the plot level (~1 ha). The combination of imaging spectroscopy with physically based radiative transfer (RT) models holds great promise for generalizing and extrapolating insights from plot-based studies to whole landscapes. Here, we tested the capacity of a simplified 3D RT approach to retrieve the structural and chemical traits of individual tree crowns (ITCs) from a highly diverse tropical forest. We first produced two datasets called measured and simulated. The measured dataset was composed of ITC reflectance extracted from sunlit imaging spectroscopy pixels. The simulated dataset was produced using a look-up-table approach and the discrete anisotropic radiative transfer (DART) model. We then compared the simulated and measured reflectances of ITCs in terms of shape difference by computing the spectral angle. The results showed small disagreements between the simulated and measured reflectances. Such differences impacted neither the spectral variability nor the spectral regions recognized as useful for species discrimination, showing that the spectral angle was a suitable measure of spectral similarity. Simulation robustness was assessed by comparing model parameters obtained by inversion to imaging spectroscopy vegetation indices and the proportion of non-photosynthetic vegetation (NPV), green photosynthetic vegetation (GV) and shade estimated within ITCs. DART canopy structural parameters were related to NPV (R^2 = 0.71), GV (R^2 = 0.78) and shade (R^2 = 0.55). DART canopy foliar parameters such as chlorophyll and carotenoids were related to the ratio of TCARI/OSAVI (R^2 = 0.80) indices and the simple ratio between reflectances at 515 nm and 570 nm (R_{515}/R_{570}) (R^2 = 0.54), respectively. Species-related differences in NPV, GV and shade were explained by variations in crown architectural characteristics. The simulation framework employed in this study can be applied to retrieve structural and chemical traits of ITCs from other areas in which high-resolution imaging spectroscopy data are available.

1. Introduction

Tropical forests are key Earth biomes. They harbor at least two-thirds of the world's terrestrial biodiversity (Gardner et al., 2009) and provide ecosystem services for humanity such as carbon (C) storage with 55% of the global forest C stock (Pan et al., 2011) and nutrient cycling with fixation of 70% of terrestrial nitrogen (Wang and Houlton, 2009). Most of our knowledge about the dynamics of tropical forests comes from field measurements performed at the plot level (~1 ha), but data that encompass broader spatial extents are needed to better understand the complex structure and functions of these important ecosystems. Remote sensing holds great promise for generalizing and

* Corresponding author.
E-mail addresses: matheus.ferreira@inpe.br (M.P. Ferreira), jean-baptiste.feret@teledetection.fr (J.-B. Féret), eloi.grau@teledetection.fr (E. Grau), jean-philippe.gastellu-etchegorry@cesbio.cnes.fr (J.-P. Gastellu-Etchegorry), yosio@dsr.inpe.br (Y.E. Shimabukuro), beto@ige.unicamp.br (C.R. de Souza Filho).

https://doi.org/10.1016/j.rse.2018.04.023
Received 14 December 2016; Received in revised form 28 March 2018; Accepted 10 April 2018
Available online 24 April 2018
0034-4257/

extrapolating insights emerging from plot-based studies to whole landscapes (Asner et al., 2015b). Plant canopy foliage exhibits multiple interactions with solar radiation from the visible to the shortwave infrared regions of the electromagnetic spectrum (VSWIR, 400–2500 nm). These interactions are related to leaf functional traits involved in the production of carbohydrates such as photosynthetic pigments (e.g., chlorophylls, carotenoids and anthocyanins) and others that provide defense against herbivory or physical hazards, such as cellulose and lignin (Wright et al., 2004). Thus, information is increasingly needed about spatial and temporal variation in canopy foliar properties related to ecosystem function and processes (Asner and Martin, 2016).

Imaging spectroscopy, also known as hyperspectral remote sensing, has proven to be a pivotal technology that can fill this need. Imaging spectroscopy has emerged as a promising way to map tropical forest canopy diversity (Féret and Asner, 2014; Laurin et al., 2014; Schäfer et al., 2016), to identify species at the individual tree crown (ITC) level (Clark et al., 2005a; Féret and Asner, 2013; Baldeck et al., 2015; Ferreira et al., 2016) and to estimate canopy chemical properties (Asner and Martin, 2009; Asner et al., 2015a, 2015b; Chadwick and Asner, 2016). Imaging spectroscopy data are acquired by sensors capable of measuring reflected radiation from the forest canopy over a spectral continuum of many narrow bands, which allows detection of subtle variations in the spectral response of tree species. Such variations are induced by canopy chemical traits and biophysical properties such as the leaf area index (LAI), but vegetation is not the only contributor to the variability in canopy reflectance: illumination, geometry of acquisition, background (understory plants, litter, soil, etc.) and atmospheric effects also influence the signal finally measured by the sensor (Asner, 1998; Huesca et al., 2016). This fact challenges our ability to retrieve canopy traits or information regarding biodiversity from imaging spectroscopy, particularly in tropical environments in which the canopy is spectrally and structurally very complex. A better understanding of diffusive and absorptive processes occurring within the canopy of tropical forests and influencing canopy reflectance is needed to address these issues. Radiative transfer models (RTMs) are valuable tools for improving our understanding of these processes and their influence on the electromagnetic signal.

RTMs are physical models that describe photon transport mechanisms acting within the canopy (leaves, branches, twigs, etc.) and the background and are capable of simulating the spectral response of forest areas. Once a physical model produces realistic simulations, it can be used to estimate biophysical and biochemical vegetation traits from canopy reflectance in different ways. RTMs are known to be more generalizable than data-driven models adjusted with measurements because they can simulate remote sensing data in a variety of acquisition and environmental conditions (Myneni et al., 2002; Verrelst et al., 2015) and are less prone to bias induced by the sampling strategy of measured data. A large number of RTMs exist, differing by their complexity and by the hypotheses upon which they rest. Operational regional monitoring requires computationally efficient RTMs and procedures applicable to satellite imagery acquired by sensors with coarse-to-moderate spatial resolution (MODIS, Thematic Mapper). Such applications usually rely on hypotheses about the homogeneity of the vegetation stand, which makes one-dimensional (1D) RTMs particularly appropriate, because they describe vegetation as a turbid medium to statistically represent light interactions in a given volume (e.g., group of leaves, atmosphere or water) (Verhoef et al., 2007; Jacquemoud et al., 2009; Houborg et al., 2015). In the case of heterogeneous canopies characterized by complex architectures, including substantial shadowing effects and variations in branching pattern, three-dimensional (3D) RTMs are more appropriate (Schneider et al., 2014; Gastellu-Etchegorry et al., 2015) because they can deal with explicitly described canopy structures. The level of details and type of information required by the existing 3D RTMs to describe this canopy structure may vary depending on the model in use and objectives pursued. A number of models featuring integration of canopy architecture have been developed (for a recent review refer to Widlowski et al., 2015), including the discrete anisotropic radiative transfer (DART) model (Gastellu-Etchegorry et al., 2015).

DART is currently one of the most comprehensive 3D RTMs and has been widely used to simulate the radiative transfer of forest canopies, helping to interpret the radiometric signal measured by remote sensors. Simulations of various types of forested ecosystems have been performed so far from alpine forests to diverse tropical forests for ecological and forestry purposes (Gastellu-Etchegorry et al., 1996; Schneider et al., 2014). These simulations comprised a wide range of remotely sensed data (including imaging spectroscopy data and very high spatial resolution data) to generate textural and spectral information. Malenovský et al. (2008) used DART to investigate the influence of woody elements on the canopy spectral response and the LAI retrieval of a Norway spruce (*Picea abies*) forest. Simulations were performed in the 450–800 nm spectral range and compared with top of canopy (TOC) reflectance acquired by an airborne imaging spectroscopy sensor. The authors highlighted the importance of including woody elements in radiative transfer-based approaches to retrieve LAI, particularly when individual tree crowns were considered. In the same study area, DART was successfully used by Malenovský et al. (2013) to retrieve leaf chlorophyll content from imaging spectroscopy. For this purpose, they simulated the imaging spectroscopy data in a spectral region sensitive to chlorophyll absorption located between 650 and 720 nm; then, they inverted the model using artificial neural networks. In tropical environments, Barbier et al. (2010) used DART to verify the relationship between canopy textural attributes and crown diameters and quantify the impact of satellite image acquisition parameters (viewing and illumination angles) on the results of the FOTO method (Couteron, 2002) that was applied to determine crown size and heterogeneity. Morton et al. (2016) used DART to build a 3D Amazon forest scene and study the diurnal and seasonal variability in light utilization. The model was parameterized with high-density light detection and ranging (LiDAR) data and in situ measurements. A realistic representation of the forest stand permitted the authors to investigate the influence of the forest structure on light interactions occurring within the canopy.

To investigate the potential and limitations of the various types of remote sensing data for applications dedicated to the retrieval of canopy chemical traits and biophysical properties of forest ecosystems using 3D RTMs, researchers require the ability to produce realistic and accurate simulations of the remote sensing signal. The realism and accuracy of these modeling tools should then be compatible with the level of details available to run the simulations. Thus, forward modeling studies are necessary to gain knowledge on model limitations, costs required for realistic simulations and photon transport mechanisms contributing to the variability in canopy reflectance. Moreover, forward modeling provides an efficient way to identify spectral regions showing high fidelity or discrepancies between measured and simulated data. This information helps to select suitable spectral ranges to be used when applying the model to retrieve a certain canopy variable and to improve the model itself (Schlerf and Atzberger, 2006; Zeng et al., 2016).

State-of-the-art 3D RTMs, such as DART, handle the description of many factors that influence the signal measured by a remote sensor. This ability makes it a powerful tool for understanding light diffusion processes that set up the radiation field of forest canopies. However, a very comprehensive description requires a large amount of information to parameterize the many parameters controlling all possible scattering mechanisms in the scene, which is usually not fully available. Therefore, performing 3D modeling of complex heterogeneous canopies requires a certain number of assumptions and trade-offs to establish the optimal description level for each factor based on available information and, importantly, to fully understand the effects resulting from default values set for variables missing experimental measurements.

To date, little is known about the performance of 3D RTMs for simulating airborne imaging spectroscopy data acquired over diverse

tropical forests. Ideally, simulating the spectral response of individual tropical trees would require a detailed parameterization of the 3D crown architecture, which can be derived from high-density airborne or terrestrial LiDAR and extensive field measurements (Morton et al., 2016; Schneider et al., 2014) combined with intensive field spectroscopy information to characterize the optical properties of each scene component (leaves, trunk, branches, understory). This process is extremely time consuming and expensive. Most studies involving 3D modeling of forests use assumptions regarding canopy architecture and optical properties when no field data or LiDAR acquisitions are available: simplified geometric shapes such as ellipsoidal volumes are used to represent trees, which are partially or completely filled with a turbid medium representing the leaves and characterized by uniform properties (density, leaf angle distribution, and leaf optical properties).

Here, we test the validity of simplified geometric representations of tropical trees and turbid description of their foliage and non-photosynthetic elements when simulating their reflectances at the canopy level. The work tests the following hypotheses: (i) information on structural and chemical properties of tropical trees can be retrieved by combining imaging spectroscopy and a simplified 3D RTM approach based on assumptions regarding crown architecture, understory vegetation, branch optical and leaf structural properties and (ii) tree species–related differences in the proportion of green vegetation (GV), non-photosynthetic vegetation (NPV) and shade are driven by crown architectural characteristics.

We designed a methodology aiming at comparing airborne imaging spectroscopy data acquired over a complex tropical forest with DART simulations obtained after application of a certain number of simplifications. This methodology was based on the generation of a look-up table (LUT) of ITC reflectance using DART simulations obtained by realistic combinations of biophysical and chemical vegetation properties as well as a simplified geometric architecture of the trees. We performed a sensitivity analysis to understand how each DART parameter affects the simulated canopy reflectance. Structural and chemical traits of ITCs were retrieved by inversion of simulations that were spectrally similar to measured data. Subsequently, the drivers of species-related differences in the proportion of GV, NPV and shade were analyzed.

2. Materials

2.1. Study area

The study area is a well-preserved tropical seasonal semi-deciduous forest located in the municipality of Campinas, São Paulo State, southeastern Brazil (22°49′13.4″S 47°06′43.6″W) (Ferreira et al., 2016). It is an old-growth forest area that is approximately 630 m a.s.l., subject to a 5-month dry season (April to September) (Leitão Filho, 1982) and characterized by deciduous and evergreen tree species. The elevation of the area ranges from 580 to 610 m. The site receives approximately 1503 mm of precipitation per year, with < 100 mm/month during the dry season. Mean annual temperature is 20.5 °C, ranging from 11 to 28.5 °C. The area has high floral diversity, with > 100 tree species per hectare (Farah et al., 2014).

2.2. Imaging spectroscopy data

Imaging spectroscopy data were acquired under clear sky conditions on June 7, 2010 using the AISA Eagle (Spectral Imaging, Inc., Oulu, Finland) sensor that covered the visible/near-infrared (VNIR, 400–970 nm) wavelength range. AISA Eagle's standard radiometric calibration was achieved with a Labsphere USS-2000-V uniform source, providing data that were within ± 5% of absolute radiance. The central wavelength locations of this output were known and certified within 0.5 nm accuracy. AISA Eagle was mounted on an aircraft that flew 1350 m above ground level at a speed of 130 kts, resulting in a spatial resolution of 1 m. The area covered comprised 251.8 ha. Ten flightlines were acquired in 28 min in the north-south direction, starting at 1:27 PM, when the sun's zenith and azimuth angles were 47.1 and 345.0°, respectively. Using a radiometric resolution of 12 bits, 122 VNIR spectral bands spaced 5 nm apart and with a full width at half maximum (FWHM) varying from 5.6 to 6.7 nm were acquired. The data collected were atmospherically and geometrically corrected according to the procedures described in Ferreira et al. (2016). Spectral bands located below 450 and above 920 nm were discarded due to their low signal-to-noise ratio (SNR). Finally, 99 bands covering the 450–920 nm spectral range were retained for further use.

Table 1
Species list, number of individual tree crowns (ITCs), mean crown size, number of pixels and diameter at breast height (DBH).

Species name	Code	ITCs	Mean crown size (pixels)	Pixels	DBH (cm)
Aspidosperma polyneuron	AP	25	112	2631	48–96
Astronium graveolens	AG	59	100	5929	30–57
Cariniana legalis	CL	50	266	13,290	52–111
Croton piptocalyx	CP	83	80	6353	35–71
Diatenopteryx sorbifolia	DS	18	21	376	49–63
Hymenaea courbaril	HC	18	210	3650	65–95
Pachystroma longifolium	PL	15	60	901	50–70

2.3. Individual tree crown dataset

The high spatial resolution of the imaging spectroscopy data permitted visualization of ITCs that were outlined throughout the study area. These ITCs were visited and identified to the species level in the field, following the approach of Ferreira et al. (2016). Seven species were identified from 268 ITCs (Table 1). Photographs of some trees were taken during the field work (Fig. 1).

3. Methods

In this section, we first describe the methodological steps used to build our measured dataset. Next, we detail the RTM strategy employed to simulate canopy reflectance with the DART model, thereby generating a simulated dataset. Then, we describe the sensitivity analysis applied to the simulated dataset to understand the influence of each parameter of interest on the final reflectance value simulated with DART. Finally, we introduce the criteria used to compare measured data with simulations and the methods used to retrieve canopy traits from measured data based on the similarity with simulated data. Fig. 2 summarizes the methodological steps applied to the retrieval of chemical and structural properties of ITCs.

3.1. Production of the measured dataset

We first extracted pixels corresponding to the manually delineated ITCs from the imaging spectroscopy data and filtered them to discard those influenced by shadows. This choice was motivated by the higher SNR ratio corresponding to sunlit pixels (Malenovský et al., 2013). We defined a threshold value for NIR (870 nm) reflectance to differentiate between sunlit and shaded pixels: pixels with NIR reflectances above 25% were defined as sunlit (Fig. 3). Finally, we averaged the reflectances corresponding to sunlit pixels for each ITC and obtained a measured dataset with 268 reflectance spectra.

3.2. Production of the simulated dataset

3.2.1. DART radiative transfer

DART is a 3D radiative transfer model that simulates radiation

Fig. 1. Individual tree crowns from species considered in the study. Photographs were taken during the dry season. Photos credit: M. P. Ferreira.

propagation in urban, agricultural and natural landscapes (Gastellu-Etchegorry et al., 2015). DART allows for the simulation of the signal acquired by various types of passive and active sensors in the optical domain, including airborne and spaceborne sensors, such as imaging spectroscopy and LiDAR sensors. A DART scene is a 3D representation of the Earth's surface characterized by a given level of details. Scenes can range from simple structures, such as turbid layers, to highly detailed 3D objects. The 3D scene is then divided into volume elements (voxels). The user can define the voxel size to optimize radiation scattering and simulate types of scene elements. The scene can contain triangles to position elements exactly (e.g., leaves, branches or walls) and/or turbid media. In a leaf voxel, leaves are represented by small plane surfaces with scattering phase functions. These functions are the sum of a Lambertian component representing radiation that penetrates the leaf and a specular component associated with radiation reflected by leaf surface (Gastellu-Etchegorry et al., 1996). A turbid medium that represents leaves inside a crown is defined by its leaf surface density (m^2/m^3), leaf angle distribution (LAD) and individual leaf optical properties (reflectance and transmittance spectra). Each voxel can be filled independently with a turbid medium and/or triangles. Further details about the DART model can be found in Gastellu-Etchegorry et al. (1996, 2015). When using a simplified geometric representation of trees, individual trees can be described as elementary geometrical shapes (conic, spherical or ellipsoidal) filled with a turbid medium containing a mix of foliage and woody elements, combined with facets (triangles) to represent the trunk. A fraction of empty voxels within the crown can also be used to add variability and induce an effect that can be compared to the clumping effect (Smolander and Stenberg, 2003). Thus, parameters defining a single tree include structural parameters (i.e., size and shape of the crown, distribution of leaves and empty cells within the crown) and optical parameters (e.g., optical properties of leaves and branches).

We employed a unique simplified representation to simulate the spectral response of trees at the ITC level: each tree was depicted as a single tree located at the center of a 10 × 10 m scene. The crown was round with a diameter of 10 m centered at a height of 20 m. This crown was voxelized to obtain 0.5 × 0.5 × 0.5 m^3 voxels filled with foliage and woody branches modeled as two separated turbid media, each medium defined by its density and optical properties. We opted for a voxel half the size of a pixel to optimize multiple scattering of leaves and branches within the crown. The proportion of full and empty voxels within the crown was also studied as a parameter influencing the tree's reflectance. Branch reflectance spectra were set to a measured bark spectrum. Each combination of branch, leaves, understory density and proportion of empty voxels resulted in a particular global scene PAI (Plant Area Index: LAI + woody elements). The forest understory was represented by a turbid plot of 2.5 m height (± 0.5 m) covering a flat ground. Standard spectra from the DART dataset were used to

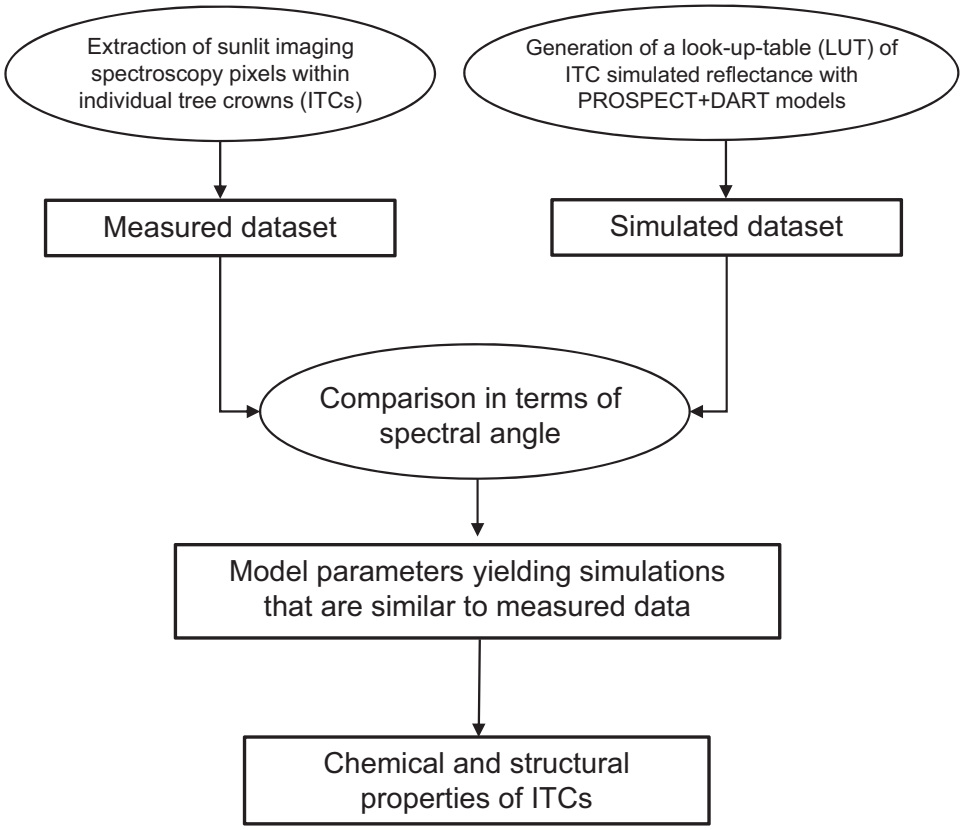

Fig. 2. The methodological steps of the study for the retrieval of chemical and structural properties of individual tree crowns (ITCs). Ellipsoidal boxes represent data processing. Rectangular boxes refer to inputs or outputs of data processing.

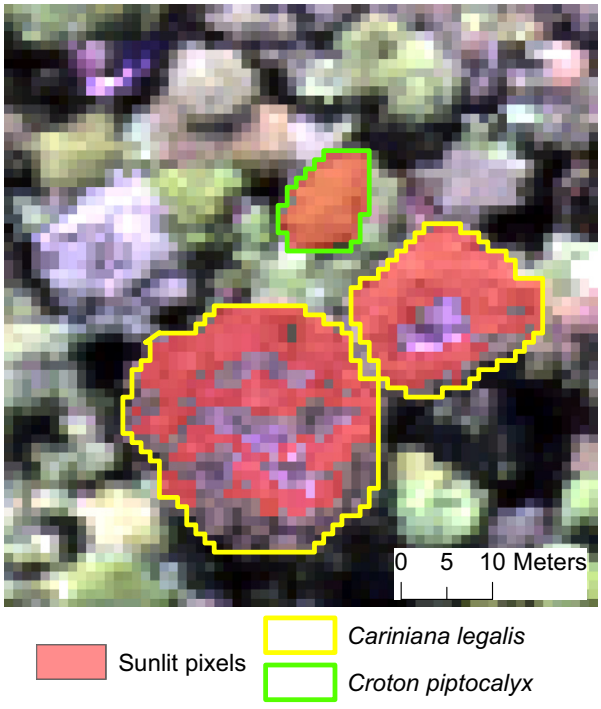

Fig. 3. Sunlit pixels selected within individual tree crowns to perform the comparison between simulated and measured reflectances. A true color composition of the imaging spectroscopy data (R = 638 nm; G = 548 nm; B = 460 nm) is shown in the background.

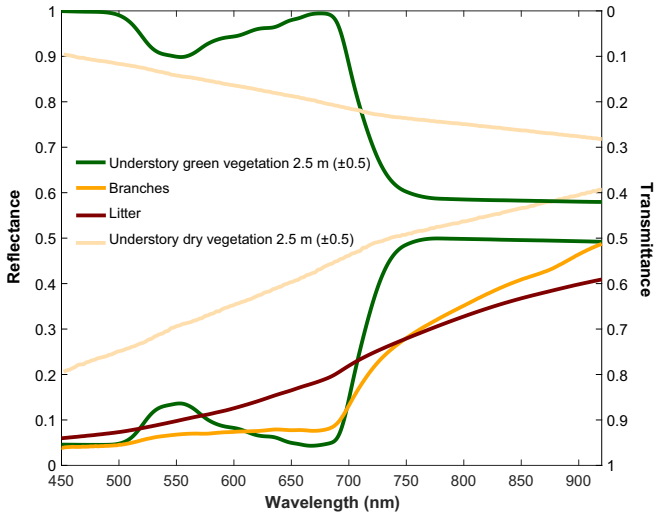

Fig. 4. Optical properties of understory green and dry vegetation up to 2.5 m (± 0.5), branches and litter used in the DART simulations.

characterize optical properties of the understory vegetation and litter (Fig. 4). Leaf optical properties were simulated with the PROSPECT-5 model (Féret et al., 2008). PROSPECT-5 simulated leaf directional-hemispherical reflectance and transmittance over the 400–2500 nm spectral range using the following input parameters: chlorophyll $a + b$ (C_{ab}, µg·cm^{-2}), carotenoids (C_{xc}, µg·cm^{-2}), equivalent water thickness (C_w, g·cm^{-2}), dry matter content (C_m, g·cm^{-2}) and the leaf structure parameter (N). The N parameter accounted for leaf anatomy.

The bidirectional reflectance factor (BRF) was modeled using a flux ray tracking approach based on the exact kernel and discrete ordinate

methods (Kimes and Kirchner, 1982; Gastellu-Etchegorry et al., 2015), in which the sun and the atmosphere were the only radiation sources. The atmosphere was simulated using a rural aerosol model with 23 km of visibility (RURAL23) and a tropical gas model derived from MODTRAN (Berk et al., 2011). Reflectance at the top of the canopy was obtained by iteratively tracking radiation fluxes along 100 discrete directions (Yin et al., 2013). Instrumental specifications of the sensor and geometry at the moment of image acquisition were set to simulate AISA Eagle images: spectral filter functions of the bands, FWHM, field of view (FOV), viewing direction, altitude and sun position. Simulations were conducted for 99 bands covering the VNIR spectral range using DART version 5.6.1 with the multithreading functionality in a UNIX environment and a fast computer (6-core processor, 64 GB RAM).

3.2.2. LUT generation

Users can set a large number of parameters in the DART model, so we selected a reasonable set of parameters to be investigated in our study. The first goal was to identify these parameters and their corresponding ranges of variation. Because our study focuses on the comparison between measured and simulated data for a single airborne acquisition, we set all variables related to atmospheric properties and geometry of acquisition to unique values (view angle = nadir; sun zenith angle = 47.1°; sun azimuth angle = 345°; tropical gas model and visibility = 23 km). The ranges of variation of the other parameters were based, whenever possible, on the literature and on our own experience, always including some extremes to ensure capture the potential boundary conditions.

The DART parameters could be divided into three main categories: canopy structural properties, leaf chemical and structural properties (corresponding to the input parameters of PROSPECT-5, described in Section 3.2.1) and scene optical properties (corresponding to scene materials other than leaves). The canopy structural properties are as follows:

- Leaf angle distribution (LAD): six functions were considered to characterize LAD, according to De Wit (1965): *planophile* (horizontal leaves were most frequent), *erectophile* (vertical leaves were most frequent), *plagiophile* (oblique leaves were most frequent), *extremophile* (oblique leaves were least frequent), *spherical* (relative frequency of leaf angle was the same as the surface elements of a sphere) and *uniform* (proportion of the leaf angle was the same at any angle). The mean leaf angle corresponding to each LAD function was as follows: 26.76° for *planophile* LAD; 63.24° for *erectophile* LAD; 45° for *plagiophile*, *extremophile* and *uniform* LAD and 57.3° for *spherical* LAD. For simplicity, leaves were treated as Lambertian surfaces.
- Density of branches per voxel (DBV): proportion of infinitely small flat surfaces with branch optical properties within voxels. This parameter accounted for non-photosynthetic vegetation within the crown.
- Density of leaves per voxel (DLV): volume density (m^2/m^3) of infinitely small flat surfaces with leaf optical properties. DLV described the green photosynthetic vegetation and leaf density within the crown.
- Proportion of full voxels within the tree crown (pVoxels): percentage of full voxels filled with leaves randomly distributed within the crown. The proportion of voxels filled with branches was fixed to 50% for all simulations. Low pVoxel values meant a high proportion of empty voxels with the crown and, consequently, an increase of internal-crown shadows.

The scene optical parameters are

- Optical reflectance factor of branches (OBF): additive offset applied to the branch spectra.
- Optical reflectance factor of the ground (OGF): additive offset applied to the ground spectra.

These parameters and their corresponding ranges of variation are summarized in Table 2. For each simulation, we opted for the random selection (uniform distribution) of a value within the ranges of variations of each parameter as shown in Table 2. Because DART simulations were computationally demanding (when compared with other simpler physical models such as the SAIL model), we generated 3500 LUT entries, which appeared a reasonable trade-off between the number of simulations and processing time.

3.3. Sensitivity analysis

Once the LUT was generated, we investigated the influence of each parameter on the spectral response of the simulated tree to identify the spectral regions most sensitive to changes in each input parameter. To achieve that goal, we performed a one-at-a-time sensitivity analysis (OAT-SA). OAT-SA consisted in varying each DART parameter one at a time by specific increments, keeping all other parameters at their base-case values (Table 2). For each simulation, we extracted TOC reflectances of all pixels within a radius of eight meters from the center of the crown, aiming to avoid mixed pixels at the border of the crown. The results of the OAT-SA were presented using the mean and standard deviation computed from reflectances of the pixels comprising the simulated tree.

3.4. Comparison between simulated and measured reflectances

The retrieval of vegetation variables from reflectance measurements using physically based approaches depended, among other things, on i) the ability of the model to generate realistic simulations and ii) the criterion defined to compute the spectral similarity. Here, we compared measured and simulated reflectances based on a shape criterion. To evaluate the suitability of this measure, we also quantified the relative importance of simulated and measured bands to differentiate among species. Our hypothesis was that spectral regions recognized as relevant for species discrimination should be the same for measured and simulated datasets if simulations were realistic. Moreover, the spectral variability computed within and among species should be similar between these datasets.

3.4.1. Shape difference

We compared simulated and measured reflectance of the ITCs using the spectral angle (θ) as a criterion for spectral similarity according to Price (1994):

$$\theta_{M,E} = \cos^{-1}\left(\frac{\int_{\lambda_a}^{\lambda_b} M(\lambda)S(\lambda)d\lambda}{\left[\int_{\lambda_a}^{\lambda_b} M(\lambda)^2 d\lambda\right]^{\frac{1}{2}}\left[\int_{\lambda_a}^{\lambda_b} S(\lambda)^2 d\lambda\right]^{\frac{1}{2}}}\right) \quad (1)$$

where $\theta_{M,E}$ is the spectral angle, measured in degrees if multiplied by $(180/\pi)$, between a given measured spectrum (M) and its simulated counterpart (S) in the spectral interval λ_a to λ_b, i.e., 450 to 920 nm. Within a given species there is a systematic offset between spectra caused by variation in amplitude, which increased the spectral variability even if the spectral shapes were the same. Variations in amplitude were caused by brightness differences and were not adequate to enhance spectral differences or to characterize the ITCs spectrally. The spectral angle, also known as the shape difference, removed the influence of the amplitude between two spectra.

The spectral angle was also a suitable measure of the spectral variability within and among species (Ferreira et al., 2016; Richter et al., 2016). Here, we were interested to know whether the spectral variability was preserved in the simulated dataset. The spectral angle was computed at two levels using all 99 VNIR bands: (*i*) within species, θ was calculated for all pairwise combinations between the reflectances

Table 2
DART + PROSPECT parameters, their ranges of variation, increments and nature used to build the look-up table (LUT) and to perform the one-at-a-time sensitivity analysis (OAT-SA).

Canopy structural parameters	Unit/Type	Range of variation	Increment LUT	Increment OAT-SA	Base-case OAT-SA	Nature
Leaf Angle Distribution (LAD)	*Planophile* *Erectophile* *Plagiophile* *Extremophile* *Spherical* *Uniform*	*Planophile* to *uniform*	–	–	*Planophile*	Categorical
Density of branches per voxel (DBV)	Volume %	0–0.25	0.25	0.25	0.25	Categorical
Density of leaves per voxel (DLV)	m^2/m^3	0.5–3	–	0.5	1.5	Continuous
Proportion of full voxels within the tree crown (pVoxels)	%	40–100	20	20	80	Categorical
Scene optical parameters						
Optical reflectance factor of branches (OBF)	–	0–1	0.5	0.5	1	Categorical
Optical reflectance factor of the ground (OGF)	–	0–1.5	0.5	0.5	1	Categorical
PROSPECT-5 parameters						
Chlorophyll $a + b$ (C_{ab})	$\mu g \cdot cm^{-2}$	10–110	–	20	30	Continuous
Carotenoids (C_{xc})	$\mu g \cdot cm^{-2}$	5–25	–	5	10	Continuous
Equivalent Water Thickness (C_w)	$g \cdot cm^{-2}$	0.002–0.042	–	0.01	0.012	Continuous
Dry Matter Content (C_m)	$g \cdot cm^{-2}$	0.003–0.033	–	0.005	0.008	Continuous
Leaf Structure (N)	–	1.4–3.4	–	0.5	1.9	Continuous

of a given species, and (*ii*) among species, θ was computed for all pairwise combinations between the reflectances of a given species and all other species, one at a time. The results were presented in two confusion matrices. One matrix showed the spectral angle within and among species based on measured data only, and the other matrix showed the spectral angle computed between simulated and measured data.

3.4.2. Feature importance

One step toward the realism of simulations is to test if measured data and corresponding simulated data share the same spectral bands of interest to discriminate among species. We used a feature importance procedure to estimate the relative importance of different spectral bands from measured and simulated reflectance to discriminate the seven species (Table 1). The aim was to verify whether spectral regions recognized as relevant to classify the species were the same on both simulated and measured data.

The random forest (RF) algorithm computes indicators of feature importance that have been widely used in remote sensing and ecology applications (Chan and Paelinckx, 2008; Cutler et al., 2007; Guo et al., 2011; Pal, 2005). RF is a tree-based ensemble classifier, i.e., it is composed of a combination of n_{tree} decision trees. The classification task is achieved by a majority vote of the output of the individual trees. To build an ensemble, RF randomly creates new training sets with replacement by resampling the original data as many times as the number of samples. At each split, the method uses only a random subset of input features, composed of m_{try} features that the user must define.

Feature importance metrics are based either on the permutation importance measure, which is also called mean decrease in accuracy (MDA), or the Gini impurity, known as the mean decrease in Gini (MDG) (Breiman, 2001). While the majority of previous studies have focused on the first, we focused on the second because it proved to be more stable and has been successfully applied to spectral data (Menze et al., 2009; Calle and Urrea, 2011). MDG is derived from the training of the RF classifier. At each decision tree node, the optimal split is sought using the Gini impurity, i.e., a measure of how well a potential split separates the samples of this particular node (Menze et al., 2009). MDG is then calculated by summing all of the decreases in Gini impurity at each node split, normalized by the number of trees (Breiman, 2001; Menze et al., 2009).

MDG was used to assess the contribution of each measured and simulated band to differentiate the species. First, based on the θ criterion, we selected the most similar simulated reflectances from the LUT to the measured reflectances. Second, we used a balanced set containing the measured spectral response of ten ITCs per species to train the RF algorithm and obtain a value of MDG per band. We selected ten ITCs per species because the RF algorithm tends to favor the majority classes (Chen et al., 2004), which can lead to erroneous results. MDG was computed 100 times changing at each realization the ITCs used to train the classifier. This procedure allowed us to consider all ITCs and avoid the problem of class imbalance. Finally, the abovementioned process was repeated using the simulated counterparts of the measured reflectances. The results were shown by the average of the MDG computed over the 100 realizations for both measured and simulated data. For this experiment, the RF parameters were set to $n_{tree} = 500$ and $m_{try} = 80$. The R packages 'randomForest' (Liaw and Wiener, 2002) and 'varSelRF' (Diaz-Uriarte, 2007) were used.

3.5. Retrieval of chemical and structural properties of individual trees

Radiative transfer models such as DART can simulate almost any reflectance spectrum depending on the range of traits (model parameters) available for simulations. Obtaining simulations that are similar to measured data does not prove that the model is suitable for the retrieval of a given vegetation variable. It is necessary to know if the underlying combinations of model parameters are realistic. In this section, we recorded the model parameters yielding simulations that were similar to measured data (smallest θ; Eq. (1)), a procedure called LUT inversion. Ideally, inverted parameters should be compared to field measurements of the traits used to parameterize the DART model. However, such data were not available for this study. Therefore, we assessed the robustness of the inverted parameters using narrow-band vegetation indices and subpixel fractions that described canopy chemical and structural properties, respectively. Finally, we demonstrated how the developed methodology could be applied to map structural and chemical characteristics of ITCs.

3.5.1. LUT inversion

Inversion of radiative transfer models consists of finding the set of model parameters that yields simulations that are spectrally similar to measured data. However, this approach is usually ill-posed. A common method to address this issue is to consider the set of parameters that generate n solutions with the lowest θ and to derive the mean value for a given parameter to estimate. The inversion was performed by averaging the DART parameters that originated the 20 spectra that are most similar to each measured spectrum (smallest θ; Eq. (1)). The inversion procedure was performed on sunlit imaging spectroscopy pixels to map structural and chemical traits of individual trees, from which field

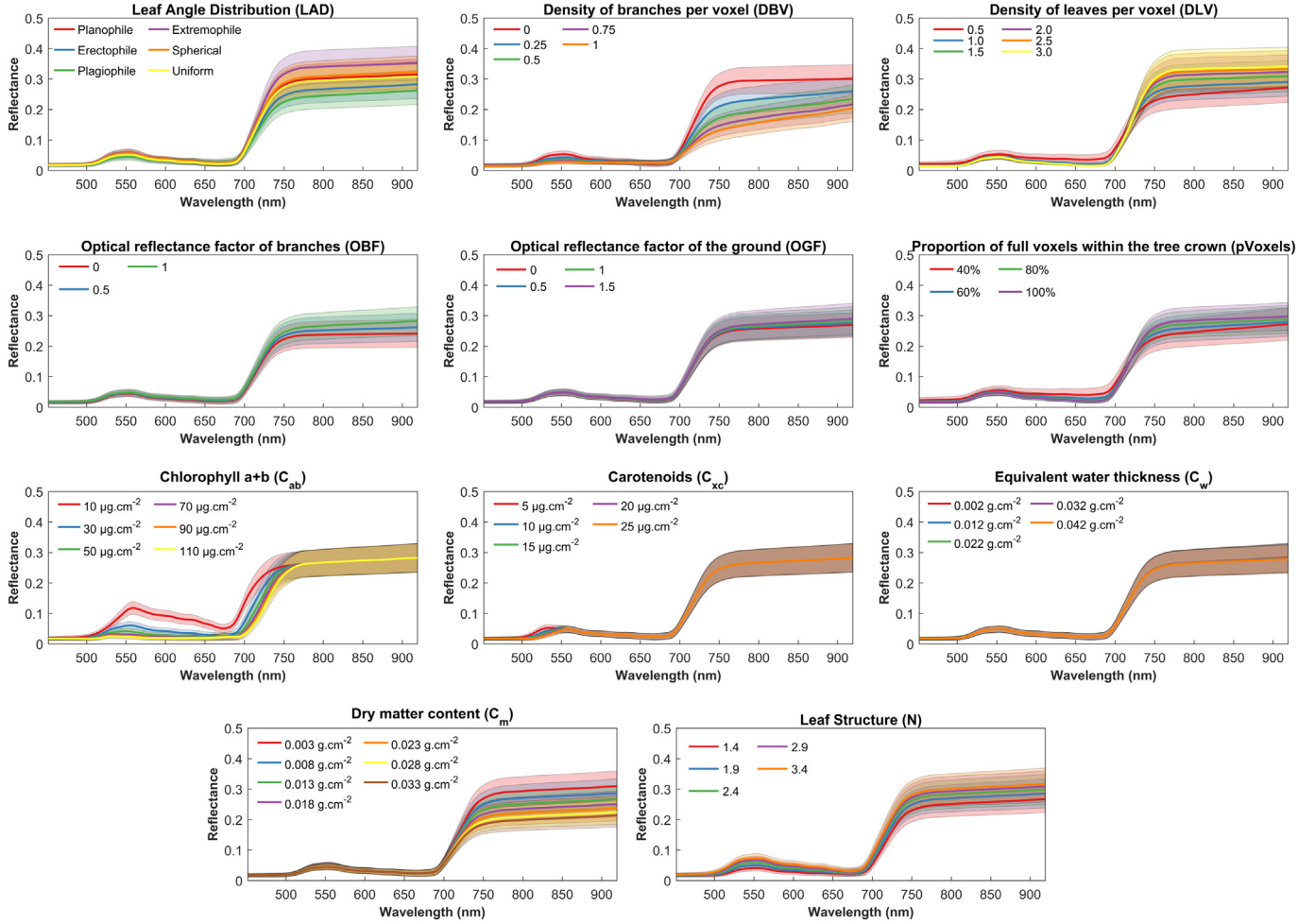

Fig. 5. Variation in the spectral response of the simulated individual tree crown after varying each DART parameter and keeping all other parameters fixed at their reference values (one at a time sensitivity analysis (OAT-SA)) (see Table 2).

photographs were available.

3.5.2. Spectral mixture analysis

The simulation approach developed in this work (Section 3.2.1) was based on a simplified tree representation with known assumptions. Specifically, crown architecture was simulated by voxels that contain branch and leaf optical properties and a proportion of empty voxels within the crown. To test whether this approach could capture species-specific differences in canopy structure, we compared DART canopy structural parameters (Table 2) obtained by inversion to the proportion of GV, NPV and shade for each ITC. The DBV, DLV and pVoxels were expected to be related to the NPV, GV and shade fractions, respectively.

The shade fraction estimated by spectral unmixing of imaging spectroscopy data proved to be related to vegetation complexity or canopy roughness (Huesca et al., 2016). Field observations revealed that tree species under consideration feature different crown architectural characteristics defined by size, shape, leaf cover and branching (Fig. 1) that might produce variations in the amount of crown-internal shadows, foliage and NPV. To quantify the proportion of GV, NPV and shade within ITCs, we performed multiple endmember spectral mixture analysis (MESMA; Roberts et al., 1998) on the imaging spectroscopy data. Spectral mixture analysis (SMA) generates linear models using a set of endmembers ("pure" spectra; Adams et al., 1993) and selects the model with the lowest root mean square error (RMSE) for each pixel. MESMA is an SMA that varies the type and number of a single class endmember (Roberts et al., 1998). First, candidate endmembers of GV and NPV were collected in the images using spatial information (coordinates collected by a GPS device) obtained in the field. Second, an SMA using three endmembers (GV, NPV and photometric shade) was performed with no constraints. The resulting fraction images were analyzed in 2D-scatterplots, used to select true GV and NPV endmembers. These image endmembers presented the highest values of their own fraction and the lowest (negative) values of the other two fractions. The final fraction images were obtained using a MESMA with the following data constraints: fraction thresholds between -0.05 and 1.05 and RMSE ≤ 0.025. The endmember fractions were constrained by a sum equal to 1.0 (i.e., spectrum 100% modeled by the endmembers) and averaged for each ITC. SMA and MESMA were run in VIPER Tools (Roberts et al., 2007). To facilitate comparison among subpixel fractions, data were normalized to the [0–1] range based on the minimum and maximum value of each fraction.

3.5.3. Narrow-band vegetation indices

Narrow-band spectral indices can provide information on biochemical properties of vegetation. We selected two indices that proved useful to the retrieval of canopy chemical traits from imaging spectroscopy data acquired in the VNIR. The first index, called TCARI/OSAVI, is sensitive to C_{ab} content and known to be less influenced by canopy background (soil) reflectance and NIR scattering caused by canopy structure. This index was proposed by Haboudane et al. (2002) and is defined as the ratio of:

$$TCARI = 3\left[(\rho_{700} - \rho_{670}) - 0.2(\rho_{700} - \rho_{550})\left(\frac{\rho_{700}}{\rho_{670}}\right)\right] \quad (2)$$

and

$$OSAVI = \frac{(1 + 0.16)(\rho_{800} - \rho_{670})}{(\rho_{800} - \rho_{670} + 0.16)} \quad (3)$$

The second index was proposed by Hernández-Clemente et al. (2012) and is related to leaf C_{xc} content of forest canopies. The index is defined as a simple ratio between reflectances at 515 nm and 570 nm and is referred to as R_{515}/R_{570}. Zarco-Tejada et al. (2013) successfully used R_{515}/R_{570} to estimate leaf C_{xc} concentration in vineyards. Here, we assessed whether model parameters describing canopy chemical traits (C_{ab} and C_{xc}) are related to TCARI/OSAVI and R_{515}/R_{570} for each ITC.

4. Results

4.1. Sensitivity analysis

The sensitivity analysis provided the opportunity to better understand how each DART parameter affected the simulated TOC spectral response (Fig. 5). The VIS range was highly influenced by the leaf optical properties. Most notably, C_{ab} variations changed the reflectance from 550 to 750 nm, which more severely impacted the green peak and the red edge. More subtly, C_{xc} and N also affected the VIS, while N impacted the entire region by increasing the amplitude of the reflectance spectra. C_{xc} produced variations only in the vicinity of 525 nm. C_m and C_w made negligible contributions to variations in the visible, with the former intensely affecting the NIR and the latter producing no variations at all. All canopy structural parameters produced remarkable changes in the NIR domain. This spectral range was more affected by LAD, DBV and DLV.

4.2. Spectral similarity

4.2.1. Shape differences between measured and simulated reflectances

Shape differences between measured reflectances and their simulated counterparts (based on minimized θ criterion; Eq. (1)) for seven species (Table 1) were small and did not exceed 1.5° of the spectral angle (Fig. 6). For comparison, the spectral angle between the understory green vegetation spectrum and the litter spectrum shown in Fig. 2 was 16°. Specifically, the mean of the spectral angle varied from 0.76° to 1.01° for *Astronium graveolens* and *Pachystroma longifolium*, respectively (Fig. 6). The shape difference distribution, which is illustrated by the width of the violin plots in Fig. 6, was highly variable for the species. For *Aspidosperma polyneuron*, the shape difference was concentrated at approximately 0.76°, while for *Diatenopteryx sorbifolia* it was more homogeneously distributed over the range of variation. This result was related to the standard deviation of the spectral angle, which reached 0.07° for *Aspidosperma polyneuron* and 0.15° for *Diatenopteryx sorbifolia*.

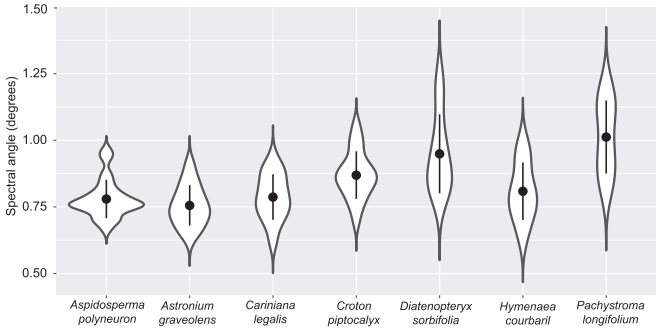

Fig. 6. Violin plots of the distribution of the spectral angle (Eq. (1)) between measured reflectances of the species and their simulated counterparts. The black dot within each violin plot represents the mean. The vertical lines above and below the mean show ± 1SD. The width of the violin plots represents frequency. Length refers to the range of variation.

Table 3
Spectral angle (in degrees) computed within (highlighted in bold) and among species based on measured data. Full species names are provided in Table 1.

Measured data		AP	AG	CL	CP	DS	HC	PL
Measured data	AP	**1.75**						
	AG	2.01	**1.77**					
	CL	1.79	1.93	**1.06**				
	CP	2.00	2.07	2.51	**1.62**			
	DS	3.30	3.56	2.28	4.21	**1.40**		
	HC	2.56	2.71	1.70	3.34	1.98	**1.90**	
	PL	2.66	2.20	3.14	1.96	4.98	4.01	**1.17**

Table 4
Spectral angle (in degrees) computed within (highlighted in bold) and among species for simulated and measured data. Full species names are provided in Table 1.

Simulated data		AP	AG	CL	CP	DS	HC	PL
Measured data	AP	**0.80**						
	AG	2.12	**0.76**					
	CL	1.93	2.01	**0.79**				
	CP	2.12	2.14	2.56	**0.87**			
	DS	3.22	3.48	2.22	4.12	**0.95**		
	HC	2.61	2.73	1.79	3.37	2.10	**0.81**	
	PL	2.39	2.00	2.87	1.85	4.73	3.76	**1.05**

Diatenopteryx sorbifolia.

Table 3 shows the within- and among-species spectral variability based on measured data. Spectral angles computed within species (diagonal of Table 3) were significantly lower than those computed among species. The highest difference regarding spectral shape was verified between *Pachystroma longifolium* (PL) and *Diatenopteryx sorbifolia* (DS) (4.98°). The lowest difference was attributed to *Hymenaea courbaril* (HC) and *Croton piptocalyx* (CL) (1.70°). Table 4 shows the spectral angles calculated between simulated and measured data. The diagonal values refer to the mean of the shape differences between measured reflectances and their simulated counterparts. The values outside the diagonal in Table 4, which refer to the spectral angle computed among species, were similar to those in Table 3. More precisely, the absolute difference between among-species spectral angles based solely on measured spectra and those computed between measured reflectances and their simulated counterparts ranged from 0.02° (HC against AG) to 0.27° (PL against AP). This result meant that simulated data were a correct proxy containing information on the spectral variability that originally existed among species.

4.2.2. Feature importance

Feature importance was performed to assess whether relevant spectral features for discriminating seven species (Table 1) were preserved in simulations. This result was confirmed by the similar patterns of the MDG obtained with simulated and measured data (Fig. 7). The RF algorithm used a limited amount of spectral information to differentiate among species. Such information was concentrated at approximately 525 nm and 725 nm and was preserved in the simulations, despite the observed shape differences between simulated and measured reflectances (Fig. 6). This result suggested that the spectral similarity measure used to compare simulated and measured data was suitable.

4.3. Sub-pixel fraction differences among species

After performing the spectral mixture analysis to obtain subpixel fractions for each ITC, we found that the proportion of NPV, GV and

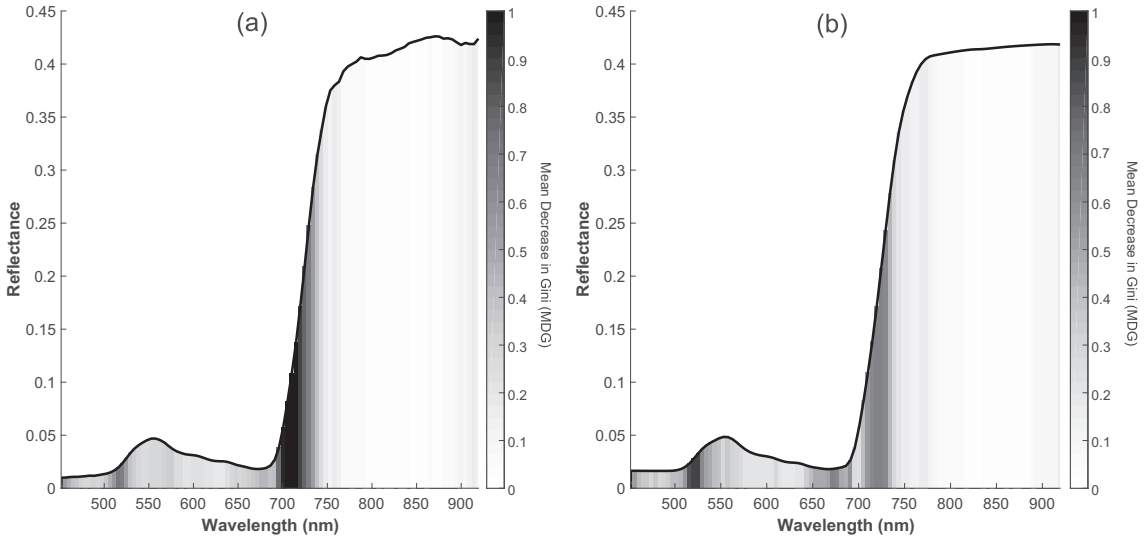

Fig. 7. Importance of the visible/near-infrared bands by MDG for discriminating trees of seven species using (a) measured reflectances of individual tree crowns (ITCs) and (b) their simulated counterparts. MDG was computed 100 times with a balanced training set with the spectral response of ten ITCs randomly selected per species. ITCs changed at each realization. The mean spectral response of *Croton piptocalyx* is plotted for clarity in (a) and (b).

shade varied among the seven species (Fig. 8). The species showed the highest separability on the NPV fraction in which only two were not statistically significantly different (Kruskal-Wallis test p-value > 0.05). The highest NPV fraction values were observed in *Diatenopteryx sorbifolia*, *Hymenaea courbaril* and *Cariniana legalis*, reaching on average 0.31, 0.30 and 0.24, respectively. For the GV fraction, four out of seven species showed statistically significant differences, with *Croton piptocalyx* corresponding to the highest value (mean of 0.62). Conversely, this species showed the lowest shade fraction values (0.4), while the highest ones were observed in *Diatenopteryx sorbifolia* and *Cariniana legalis* (0.71 and 0.67, respectively). Considering ITCs for all species, an inverse pattern was found between the GV and shade fractions (Fig. 9a) and a positive relationship was found between shade and NPV (Fig. 9b), indicating that the crown's shaded areas were attributed to NPV.

4.4. LUT inversion

4.4.1. Relationships between subpixel fractions and DART canopy structural parameters

The DART canopy structural parameters that yielded simulations that were similar to measured data (smallest θ values; Eq. (1)) were related to subpixel fractions of NPV, GV and shade, which were estimated for each ITC using a spectral mixture analysis of imaging spectroscopy data (Fig. 10). The DBV and the DLV were positively related to the proportions of NPV and GV within the crowns, respectively (Fig. 10a,b). Conversely, the pVoxels was negatively related to the shade fraction (Fig. 10c). A small value of pVoxels meant a high proportion of empty voxels within the simulated tree crown, which increased the frequency of gaps and internal-crown shadows. The DBV and DLF parameters controlled, respectively, the proportion of non-photosynthetic (branches) and green photosynthetic (leaves) material within the simulated tree. Strong positive relationships between these parameters and the NPV and GV fractions computed for measured ITCs (Fig. 10a,b) showed that model parameters obtained by inversion were

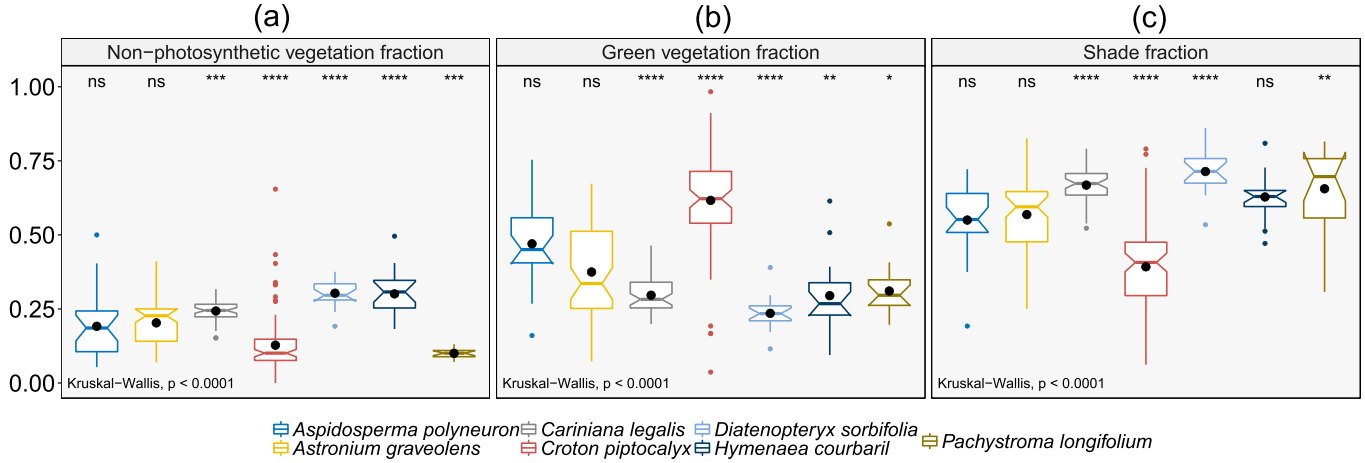

Fig. 8. Notched boxplots showing the variability of subpixel fractions among individual tree crowns of seven species (Table 1). (a) Non-photosynthetic vegetation fraction, (b) green vegetation fraction and (c) shade fraction. The central lines within each box are the medians, and the black dots are the means. The upper and lower quartiles are represented by the boxes' edges. The Kruskal-Wallis test (Theodorsson-Norheim, 1986) was performed to assess differences among species. The global p-values of the Kruskal-Wallis test are shown in the lower left corner of each panel, while the resulting p-values from multiple comparisons are represented above each boxplot. 'ns' = non-significant (p-value > 0.05); '*': p-value ≤0.05; '**': p-value ≤0.01; '***': p-value ≤0.001 and '****': p-value ≤0.0001.

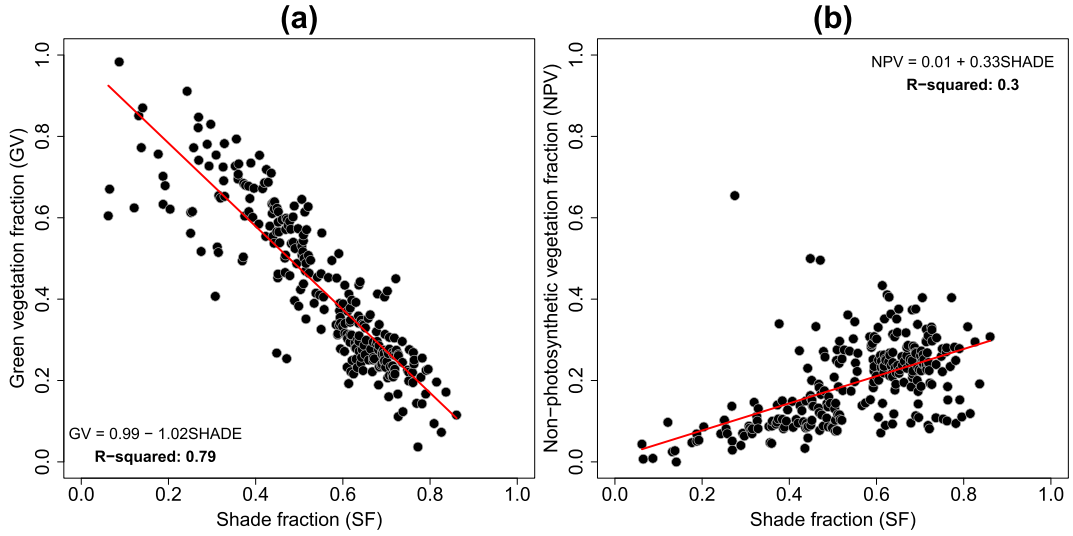

Fig. 9. Relationships between the shade fraction with the green vegetation fraction (a) and with the non-photosynthetic vegetation fraction (b) for each tree crown (black dots). Sub-pixel fractions were obtained by spectral mixture analysis of the imaging spectroscopy data.

realistic.

4.4.2. Relationships between vegetation indices and DART canopy foliar parameters

Inversion of DART simulations (Section 3.5.1) revealed that canopy foliar parameters were related to vegetation indices that were computed with the imaging spectroscopy bands for each ITC (Fig. 11). The data points of the scatter plots in Fig. 11 represented the mean values (and respective standard deviations) of the C_{ab} and C_{xc} parameters yielding the 20 most similar (smallest θ values; Eq. (1)) simulated reflectances to each measured reflectance. The standard deviation varied from 5.8 to 9.4 $\mu g \cdot cm^{-2}$ for C_{ab} and from 1.6 to 2.3 $\mu g \cdot cm^{-2}$ for C_{xc}. Previous studies showed that TCARI/OSAVI and R_{515}/R_{570} were negatively related to C_{ab} and C_{xc}, respectively (Zarco-Tejada et al., 2013; Hernández-Clemente et al., 2012). The relationship between these indices and DART parameters obtained by inversion revealed that LUT entries underlying simulations were valid.

The C_{ab} varied from 34.2 to 78.6 $\mu g \cdot cm^{-2}$, with *Pachystroma longifolium* reaching the highest values (mean of 76.4 $\mu g \cdot cm^{-2}$) (Fig. 12a). C_{xc} varied from 14.6 to 18.8 $\mu g \cdot cm^{-2}$, with lowest and highest mean values attributed to *Hymenaea courbaril* (mean of 16.2 $\mu g \cdot cm^{-2}$) and *Croton piptocalyx* (mean of 17.9 $\mu g \cdot cm^{-2}$), respectively. In general, pigment concentration among ITCs of a given species was highly variable, except for *Pachystroma longifolium*, in which the difference between the upper and lower quartiles was only 1.4 $\mu g \cdot cm^{-2}$ for C_{ab} (Fig. 12a) and 0.2 $\mu g \cdot cm^{-2}$ for C_{xc} (Fig. 12b).

4.4.3. Map of structural and chemical traits

An example map of the structural and chemical traits obtained by inversion of the DART model on sunlit imaging spectroscopy pixels is displayed in Fig. 13. Photographs taken in the field of representative trees corroborated the results of model inversion. For example, *Croton piptocalyx* featured a fully foliated crown (Fig. 13a) and a high density of leaves per voxel (Fig. 13e). Conversely, the density of branches per voxel was low in this species (Fig. 13d). *Cariniana legalis* usually has large crowns (> 20 m in diameter), low leaf cover and exposed branches (Fig. 1 and Fig. 13a). These characteristics agreed with inversion results that showed high densities of branches and low densities of leaves per voxel for *Cariniana legalis* ITCs.

5. Discussion

5.1. Simulation of the spectral response of ITCs

The sensitivity analysis provided a general overview of the influence of each DART parameter on the simulated reflectance, which was

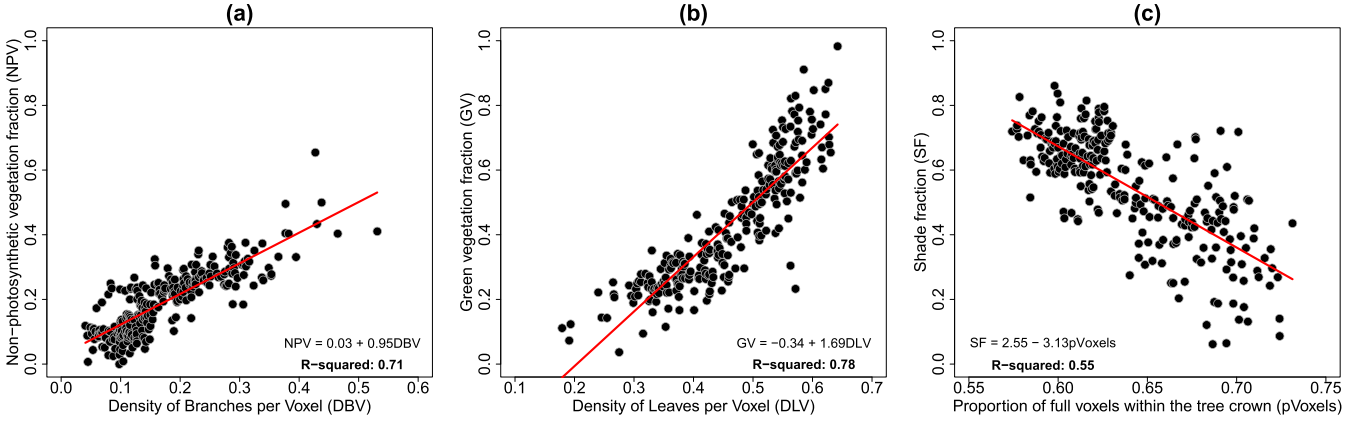

Fig. 10. Relationships between DART canopy structural parameters and subpixel fractions estimated with spectral mixture analysis of the imaging spectroscopy data. (a) Relationship between the non-photosynthetic vegetation fraction (NPV) and the density of branches per voxel (DBV). (b) Relationship between the green vegetation fraction (GV) and the density of leaves per voxel (DLV). (c) Relationship between the shade fraction (SF) and the proportion of full voxels within the tree crown (pVoxels).

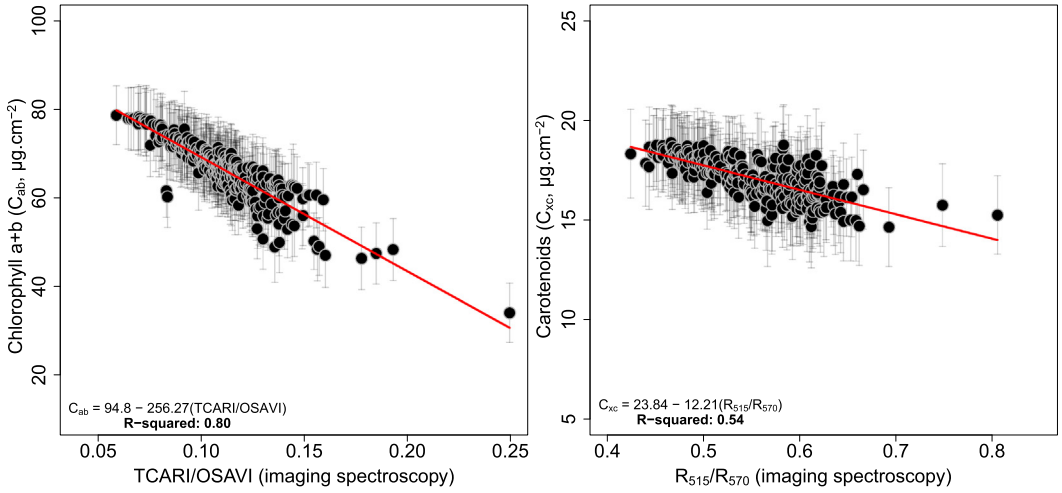

Fig. 11. (a) Relationship between the TCARI/OSAVI ratio (Eqs. (2) and (3)) computed from imaging spectroscopy and chlorophyll $a + b$ (C_{ab}) content obtained by inversion of the DART model. (b) Relationship between the R_{515}/R_{570} ratio computed from imaging spectroscopy and carotenoid (C_{xc}) content obtained by inversion of the DART model. Each point represents the mean (and associated ± 1SD bars) of the C_{ab} or C_{xc} parameter that yielded the 20 most similar simulated reflectances to each measured reflectance of the individual tree crowns.

important for assessing the 3D radiative transfer approach employed. For example, Malenovský et al. (2013) showed that the most suitable spectral region for the retrieval of canopy chlorophyll was located between 550 nm and 750 nm. The sensitivity analysis revealed that top of canopy reflectances in this spectral range were highly affected by systematic changes in the C_{ab} parameter (Fig. 5). This result meant that the simulation framework correctly modeled variations in canopy reflectance caused by chlorophyll content. Similarly, sensitivity analysis results showed that the C_{xc} parameter influenced the simulated canopy reflectance at approximately 525 nm (Fig. 5). The role played by leaf carotenoids on reflectance at this waveband has been demonstrated in previous works (e.g., Gitelson et al., 2002; Zarco-Tejada et al., 2013). Moreover, from the leaf level, canopy reflectance was sensitive to variations on N and C_m (Fig. 5), which supported the findings of Xiao et al. (2014).

The observed influence of canopy structural parameters was also corroborated by the literature. The DBV parameter increased reflectance when its value decreased to approximately zero (Fig. 5), which is a pattern that was also verified by Asner (1998) when observing the effects of woody stem material on canopy reflectance. Malenovský et al. (2008) studied the influence of woody elements on DART-simulated canopy reflectance and found that high light absorbance by woody elements decreased NIR reflectance, which agreed with the DBF pattern observed here. The DLF and LAD parameters also affected canopy reflectance, particularly in the NIR domain (Fig. 5), which concurred with previous study results (Asner, 1998; Schneider et al., 2014).

The impact of the pVoxels was noteworthy. When it reached 100%, which meant the crown had no empty voxels, the reflectance values increased. This result was expected because a higher number of voxels filled with foliage and woody material enhanced multiple scattering and increased the amount of radiance leaving the crown.

The shape differences between measured reflectances and their simulated counterparts did not exceed 1.5° in spectral angle (Fig. 6). These differences did not significantly impact either the spectral variability or relevant spectral regions for species discrimination (Fig. 7), which also confirmed that the spectral angle was a suitable measure of spectral similarity.

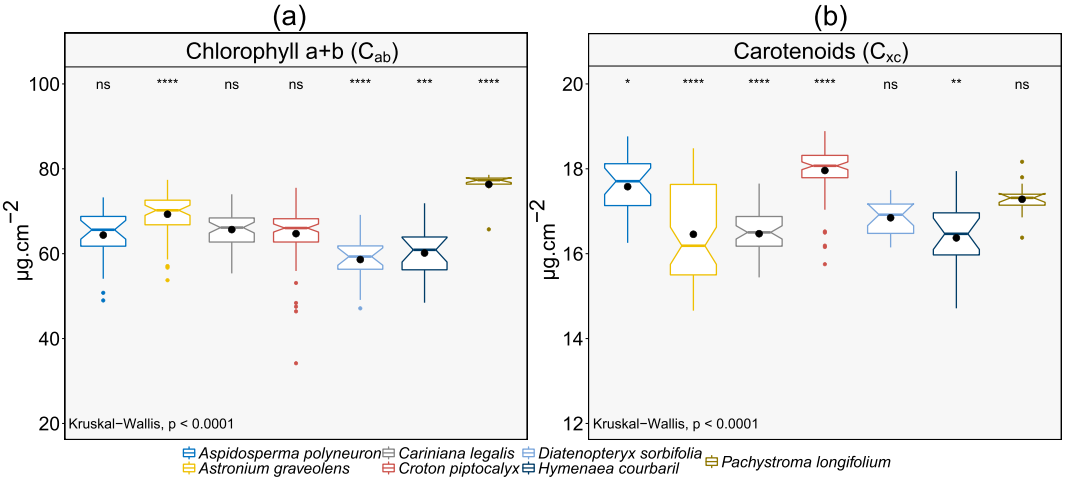

Fig. 12. Notched boxplots showing variable (a) chlorophyll $a + b$ (C_{ab}) and (b) carotenoids (C_{xc}) contents in individual tree crowns of seven species (Table 1) obtained by inversion of the DART model on imaging spectroscopy data. The central line within each box represents the median, and the black dots are the means. The upper and lower quartiles are represented by the edges of the boxes. The Kruskal-Wallis test was performed to assess differences among species. The global p-values of the Kruskal-Wallis test are shown in the lower left corner of each panel, while the resulting p-values from multiple comparisons are represented above each boxplot. 'ns' = non-significant (p-value > 0.05); '*': p-value ≤0.05; '**': p-value ≤0.01; '***': p-value ≤0.001 and '****': p-value ≤0.0001.

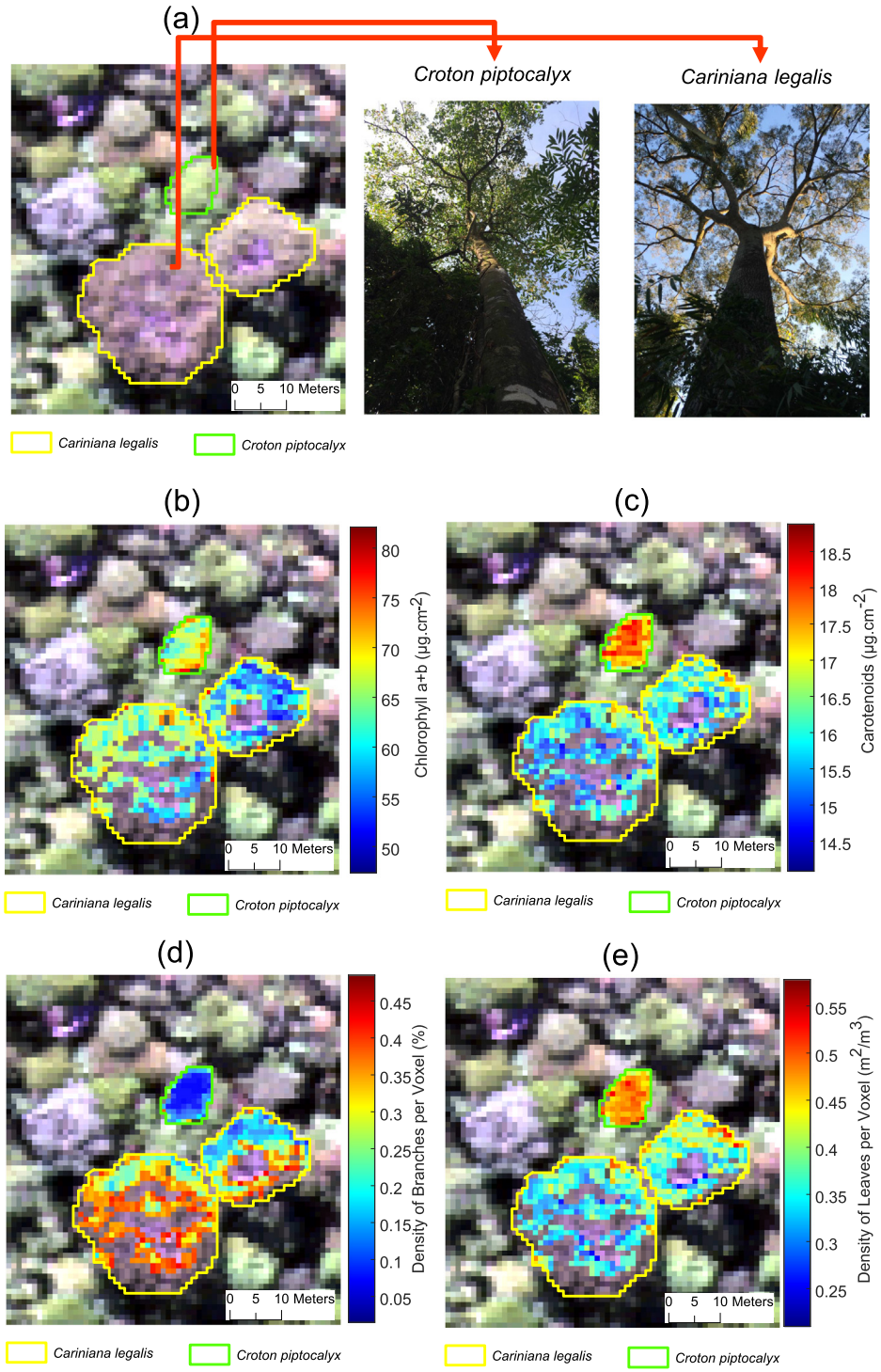

Fig. 13. Maps of chemical and structural traits of individual tree crowns obtained by inversion of the DART model on sunlit imaging spectroscopy pixels. (a) True color composition of the imaging spectroscopy data (R = 638 nm; G = 548 nm; B = 460 nm) and photographs of *Croton piptocalyx* and *Cariniana legalis* taken in the field (photos credit: M. P. Ferreira); (b) Chlorophyll $a + b$ content; (c) Carotenoid content; (d) Density of leaves per voxel; and (e) Density of branches per voxel.

The feature importance procedure (Section 3.4.2) revealed that bands located approximately at 525 nm and 725 nm provided information to classify the species. Previous research showed that these wavelengths were useful for retrieving leaf biochemical pigments (e.g., Gitelson et al., 2002; Malenovský et al., 2013), particularly carotenoids and chlorophylls, suggesting that they might drive species discrimination. However, further investigation was required to better assess the utility of the selected bands because they may differ depending on the machine learning algorithm used (Fassnacht et al., 2016). Here, the feature importance measure of random forest was employed only to verify whether relevant spectral features were preserved in simulations. Even if other bands were selected by another method, spectral regions recognized as relevant to separate the species were expected to remain largely unchanged when simulated and measured data were compared.

The simulation framework employed in this work was based on assumptions regarding crown architecture, understory vegetation, branch optical and leaf structural properties. Architecture refers to the overall shape of the crown and the spatial distribution of its elements

(e.g., branching pattern and foliage arrangement). The crown architecture of a tropical tree is complex and depends on several factors, such as its position in the forest canopy, neighboring trees, species and height (Poorter et al., 2006). Understory vegetation is characterized by juveniles of canopy trees and a wide range of small trees, shrubs and herbs in all life stages (Wright, 2002). In the tropics, leaves often have specular reflectance caused by wax layers or trichomes, which significantly influence the reflectance spectra (Levizou et al., 2005). Additionally, bark properties vary due to structural differences among species (presence of cavities and lenticels) or external influences such as lichen cover (Clark, 2009).

In our study, the simulated tropical tree featured a simple crown architecture defined by a round shape and a diameter of 10 m (Section 3.2.1). The branching pattern and foliage arrangement were modeled using structural parameters such as DBF, DLV, LAD and pVoxels. The optical properties of understory vegetation and branches were set using a standard vegetation spectrum from the DART database and a measured bark spectrum, respectively. Leaves were assumed to be Lambertian surfaces on which incidental light was equally reflected in all directions. These assumptions tended to be over-simplistic for highly diverse tropical forests, but they were necessary to model these complex environmental radiation fields, particularly when field information was limited or not available. Future work involves incorporating the spectral response of different types of branches and understory vegetation in the simulation framework. We also intend to associate a specular component with simulated radiation reflected by leaf surface types. Moreover, terrestrial laser scanning and high-resolution images acquired by unmanned aerial vehicles (UAVs) could be used to characterize crown architecture (e.g., Morsdorf et al., 2018).

5.2. Retrieval of chemical and structural properties

Our first hypothesis was that the simplified 3D RTM approach employed, when combined with imaging spectroscopy data, can be used for the retrieval of structural and chemical properties of individual trees. This notion was supported by the LUT inversion results (Section 4.4). Subpixel fractions were strongly related to DART canopy structural parameters obtained by inversion (Fig. 10). Previous investigations have shown that subpixel fractional abundance of GV, NPV and shade were correct proxies for canopy structure (Clark, 2005; Bohlman, 2008; Huesca et al., 2016), as they were related to the green leaves, bark and roughness of the crown, respectively. DART canopy foliar parameters obtained by inversion were related to narrow-band vegetation indices (Fig. 11). These indices were designed and validated specifically to retrieve biochemical compounds. TCARI/OSAVI proved useful for canopy chlorophyll retrieval in a range of vegetation types (Haboudane et al., 2002; Albrechtova et al., 2008; Zarco-Tejada et al., 2013), whereas the capacity of the R_{515}/R_{570} index to estimate leaf carotenoid content was demonstrated by Hernández-Clemente et al. (2012) and Zarco-Tejada et al. (2013).

By relating subpixel fractions and narrow-band vegetation indices (derived from the imaging spectroscopy data) to DART parameters (obtained by inversion), we proved that model parameterization underlying simulations of the spectral response of ITCs is rather realistic. We recognize, however, that a straightforward validation is required to assess the accuracy of the inversions. This result can be achieved solely with field and imaging spectroscopy data acquired synchronously, because of the rapid changes in the ITCs' biochemical and biophysical properties.

The robustness of simulations was also corroborated by field observations of individual trees, as shown in Fig. 13. The true color composition of the imaging spectroscopy data revealed a high diversity of colors (Fig. 13a), which were related to spectral differences arising from vegetation biochemical and biophysical properties. *Croton piptocalyx* showed vivid green tones due to its fully leaved crown. Conversely, ITCs of *Cariniana legalis* were characterized by purplish tones caused by low leaf cover and a high proportion of exposed branches. These characteristics agreed with results of model inversion that showed high DLV and DBV for *Croton piptocalyx* and *Cariniana legalis*, respectively. More research is needed to understand the physical meaning of these parameters and their relation to known biophysical variables, such as LAI and PAI.

Our study was based on imaging spectroscopy data acquired in the VNIR. Nevertheless, important plant properties could be retrieved from shortwave infrared (SWIR, 1000–2500 nm) reflectance. In a recent work performed in the study area, Ferreira et al. (2016) showed that SWIR information increased the classification accuracy of the species by up to 10%. The authors highlighted the relevance of bands centered at 1700 nm and at approximately 2100 and 2300 nm, which were related to the concentration of non-pigment biochemical constituents such as nitrogen, cellulose and lignin. An additional interesting research opportunity would be to test the developed simulation framework on imaging spectroscopy data acquired in the SWIR. This process could better characterize the spectral response of the ITCs and possibly reduce the ill-posed problem of model inversions. Moreover, the retrieval might be possible of important canopy foliar traits such as the equivalent water thickness and specific leaf area.

Some issues might arise when simulating remote sensing data in the SWIR. For example, the signal-to-noise ratio in this spectral region was lower than in the VNIR due to effects of atmospheric water vapor absorption. Moreover, the solar radiance is weaker from short to long wavelengths, thereby reducing the signal measured by the sensor in the SWIR. Such effects could alter the spectral shape, which impacted the comparison between simulated and measured reflectance. Finally, VNIR and SWIR data should be acquired with a single optics imager to avoid distortions in the reflectance spectrum caused by two detector arrays and instantaneous fields of view (IFOVs).

5.3. Differences in imaging spectroscopy subpixel fractions among species

The proportions of GV, NPV and shade estimated within ITCs varied among the investigated species (Fig. 8). Such differences could be explained by the crown architecture. For example, *Cariniana legalis* and *Hymenaea courbaril* showed high NPV fraction values (Fig. 8a). Field observations (Fig. 1) revealed that these species usually feature large crowns (> 15 m in diameter) with thick branches emerging from the main tree stem. This feature, combined with the low leaf density, made the spectral response of such branches more prone to being detected by the imaging spectroscopy sensor, thereby increasing the NPV fraction of these species. The presence of large branches also contributed to the amount of internal-crown shadows, producing high shade fraction values (Fig. 8c).

Diatenopteryx sorbifolia was another species featuring high NPV fraction values. The species was found in a monospecific patch in the study area, with trees forming a well-defined deciduous canopy 25 to 30 m high (Nave, 1999). During the dry season, leaf cover was low, and the sparse and short (< 4 m tall) understory layer allowed detection of reflected sunlight from the forest floor, which was composed mainly of litter (non-photosynthetic material). *Aspidosperma polyneuron*, *Astronium graveolens* and *Croton piptocalyx* showed the highest GV fraction values (Fig. 8b). This result was usually related to the fully foliated crowns of these species, as revealed by field observations (Fig. 1). These species also presented intense leaf flushing during the dry season (Morellato, 1991), particularly *Croton piptocalyx* and *Astronium graveolens*, which explained the high variability of the GV fraction among ITCs.

Differences in canopy chemical traits among species were also observed (Fig. 12). Most interestingly, *Pachystroma longifolium* showed a very peculiar pattern, reaching high C_{ab} values (Fig. 12a) with relatively low variability. This result probably arose from its dark green leathery leaves with high chlorophyll contents (Alcalá, 2010). Moreover, *Pachystroma longifolium* is an evergreen species that forms dense

monospecific patches over the study area (Gandolfi et al., 2007). The other species showed highly variable pigment concentrations among ITCs, which challenged our ability to separate them based only on these traits.

As detailed above, species-related differences in imaging spectroscopy subpixel fractions were driven by crown architectural characteristics, supporting our second hypothesis. The number of species investigated in our study was limited in comparison to the number of species found in the area (> 100 per hectare). Moreover, the high plasticity of structural and chemical traits among ITCs of a given species made their separation based on traits (either structural or chemical) very unlikely. However, as noted by Fassnacht et al. (2016), most studies focused on improving the classification accuracy without examining the vegetation traits that cause variations on the remote sensing signal and, thereby, enable species detection. The use of imaging spectroscopy data could be improved by understanding vegetation traits that affect species discrimination. For example, airborne acquisitions can be scheduled to a given season when the target species are more prone to be detected (i.e., with the presence or absence of leaves). Here, we showed that crown architecture and branching pattern influence the NPV fraction and are important traits for identifying emergent trees such as *Cariniana legalis* and *Hymenaea courbaril*, two endangered species logged heavily due to their high wood quality.

6. Conclusions and outlook

In this study, we tested the capacity of a simplified 3D radiative transfer approach—based on assumptions regarding crown architecture, understory vegetation, branch optical and leaf structural properties—to simulate the spectral response and retrieve structural and chemical traits of individual trees from a highly diverse tropical forest area. The observed variations in the simulated canopy reflectance, which were caused by systematic changes in DART parameters (one at a time sensitivity analysis), were corroborated by the literature. Measured reflectance from 268 ITCs gathered from seven species showed small differences from their simulated counterparts. Such differences impacted neither the spectral variability nor spectral regions recognized as important for species discrimination. Therefore, the spectral angle used to compare simulated and measured reflectance proved to be a useful criterion of spectral similarity. Simulation realism was assessed by comparing model parameters obtained by inversion to imaging spectroscopy subpixel fractions and narrow-band vegetation indices. Our findings revealed that species-related differences in the proportion of NPV, GV and shade are driven by crown architectural characteristics.

The methodology developed in this study for the retrieval of canopy structural and chemical traits could be applied to other areas in which high-resolution imaging spectroscopy data are available. The simulation framework was designed to reproduce the spectral response of the canopy at the ITC level. Thus, the spatial resolution of the imaging spectroscopy data should be sufficient to comprise several pixels within the tree crowns. Soon, the methodology will be applied to imaging spectroscopy data acquired using a UAV. These platforms are capable of collecting images featuring a submetric spatial resolution. Tree crown delineation algorithms can be applied to images to improve the spectral signatures of tree species by reducing spectral mixing effects.

Finally, the presented approach has the potential for mapping functional diversity over large areas. Functional diversity can be measured by combining multiple functional traits (e.g., Schneider et al., 2017), such as photosynthetic pigments (chlorophylls and carotenoids), and are key to understanding ecosystem functioning. For example, photosynthetic pigments play a prominent role in the production of carbohydrates in the leaves, since they are responsible for light capture and utilization. Plants are able to accumulate carbohydrates in the form of woody tissues in a process known as terrestrial net primary production (NPP), which has a significant role in the global carbon cycle (Ito, 2011).

Acknowledgments

This work was supported by the São Paulo Research Foundation (FAPESP) (grants n°. 2013/11.589-5, n°. 2015/50484-0 and n°. 2016/24977-1 to MPF), by the Coordination for the Improvement of Higher Education Personnel (CAPES) (grant n°. 3424/2015-04 to MPF) and by the Brazilian National Council for Scientific and Technological Development (CNPq) (grant n°. 303563/2008-7 to CRSF and grant n°. 301190/2013-5 to YES). We thank FotoTerra Atividades de Aerolevantamentos Ltda. for kindly providing the imaging spectroscopy data used in this research. JBF and EG were funded by the HyperTropik project (TOSCA program grant of the French Space Agency, CNES). We thank Dra. Cibele Hummel do Amaral for valuable assistance on the spectral mixture analysis. We gratefully thank the Editor and the Anonymous Reviewers for their insightful comments and highly constructive criticisms that improved the content and presentation of the study.

References

Adams, J.B., Smith, M.O., Gillespie, A.R., 1993. Imaging spectroscopy: Interpretation based on spectral mixture analysis. In: Pieters, C.M., Englert, P.A.J. (Eds.), Remote Geochemical Analysis: Elemental and Mineralogical Composition. Press Syndicate of the University of Cambridge, New York.

Albrechtova, J., Seidl, Z., Aitkenhead-Peterson, J., Lhotáková, Z., Rock, B.N., Alexander, J.E., Malenovský, Z., McDowell, W.H., 2008. Spectral analysis of coniferous foliage and possible links to soil chemistry: are spectral chlorophyll indices related to forest floor dissolved organic C and N? Sci. Total Environ. 404, 424–432.

Alcalá, M., 2010. Ecologia da População de Pachystroma Longifolium (NESS). I.M. Johnst. em Área Fragmentada de um Remanescente de Mata Atlântica. Master dissertation (Ecology and Natural Resources). UFSCAR, São Carlos, Brasil.

Asner, G.P., 1998. Biophysical and biochemical sources of variability in canopy reflectance. Remote Sens. Environ. 64, 234–253.

Asner, G.P., Martin, R.E., 2009. Airborne spectranomics: mapping canopy chemical and taxonomic diversity in tropical forests. Front. Ecol. Environ. 7, 269–276.

Asner, G.P., Martin, R.E., 2016. Spectranomics: emerging science and conservation opportunities at the interface of biodiversity and remote sensing. Glob. Ecol. Conserv. 8, 212–219.

Asner, G.P., Anderson, C.B., Martin, R.E., Tupayachi, R., Knapp, D.E., Sinca, F., 2015a. Landscape biogeochemistry reflected in shifting distributions of chemical traits in the Amazon forest canopy. Nat. Geosci. 8, 567–573.

Asner, G.P., Martin, R.E., Anderson, C.B., Knapp, D.E., 2015b. Quantifying forest canopy traits: imaging spectroscopy versus field survey. Remote Sens. Environ. 158, 15–27.

Baldeck, C.A., Asner, G.P., Martin, R.E., Anderson, C.B., Knapp, D.E., Kellner, J.R., Wright, S.J., 2015. Operational tree species mapping in a diverse tropical forest with airborne imaging spectroscopy. PLoS One 10, e0118403.

Barbier, N., Couteron, P., Proisy, C., Yadvinder, M., Gastellu-Etchegorry, J.-P., 2010. The variation of apparent crown size and canopy heterogeneity across lowland Amazonian forests. Glob. Ecol. Biogeogr. 19, 72–84.

Berk, A., Anderson, G.P., Acharya, P.K., Shettle, E.P., 2011. MODTRAN® 5.2. 2 User's Manual. Spectral Sciences. Inc., Burlington, MA, pp. 69.

Bohlman, S., 2008. Hyperspectral remote sensing of exposed wood and deciduous trees in seasonal tropical forests. In: Kalacska, M., Sánchez-Azofeifa, G.A. (Eds.), Hyperspectral Remote Sensing of Tropical and Sub-Tropical Forests. CRC Press, Boca Raton, FL, pp. 177–192.

Breiman, L., 2001. Random forests. Mach. Learn. 45, 5–32.

Calle, M.L., Urrea, V., 2011. Letter to the editor: stability of random forest importance measures. Brief. Bioinform. 12, 86–89.

Chadwick, K.D., Asner, G.P., 2016. Organismic-scale remote sensing of canopy foliar traits in lowland tropical forests. Remote Sens. 8, 87.

Chan, J.C.W., Paelinckx, D., 2008. Evaluation of random forest and adaboost tree-based ensemble classification and spectral band selection for ecotope mapping using airborne hyperspectral imagery. Remote Sens. Environ. 112, 2999–3011.

Chen, C., Liaw, A., Breiman, L., 2004. Using Random Forest to Learn Imbalanced Data. University of California, Berkeley.

Clark, M.L., 2005. An Assessment of Hyperspectral and Lidar Remote Sensing for the Monitoring of Tropical Rain Forest Trees. Doctoral Dissertation. University of California, Santa Barbara, CA.

Clark, M.L., 2009. Identification of canopy species in tropical forests using hyperspectral data. In: Thenkabail, P.S., Lyon, J.G., Huete, A. (Eds.), Hyperspectral Remote Sensing of Vegetation. CRC Press, Boca Raton, pp. 423–444.

Clark, M.L., Roberts, D.A., Clark, D., 2005. Hyperspectral discrimination of tropical rain forest tree species at leaf to crown scales. Remote Sens. Environ. 96, 375–398.

Couteron, P., 2002. Quantifying change in patterned semi-arid vegetation by Fourier analysis of digitized aerial photographs. Int. J. Remote Sens. 23, 3407–3425.

Cutler, D.R., Edwards, T.C., Beard, K.H., Cutler, A., Hess, K.T., Gibson, J., Lawler, J.J., 2007. Random forests for classification in ecology. Ecology 88, 2783–2792.

De Wit, C.T., 1965. Photosynthesis of Leaf Canopies. No. 663. Pudoc.
Diaz-Uriarte, R., 2007. GeneSrF and varSelRF: a web-based tool and R package for gene selection and classification using random forest. BMC Bioinf. 8, 1–7.
Farah, F.T., Rodrigues, R.R., Santos, F.A.M., Tamashiro, J.Y., Shepherd, G.J., Siqueira, T., Batista, J.L.F., Manly, B.J.F., 2014. Forest destructuring as revealed by the temporal dynamics of fundamental species–case study of Santa Genebra Forest in Brazil. Ecol. Indic. 37, 40–44.
Fassnacht, F.E., Latifi, H., Stereńczak, K., Modzelewska, A., Lefsky, M., Waser, L.T., ... Ghosh, A., 2016. Review of studies on tree species classification from remotely sensed data. Remote Sens. Environ. 186, 64–87.
Féret, J.B., Asner, G.P., 2013. Tree species discrimination in tropical forests using airborne imaging spectroscopy. IEEE Trans. Geosci. Remote Sens. 51, 73–84.
Féret, J.B., Asner, G.P., 2014. Mapping tropical forest canopy diversity using high-fidelity imaging spectroscopy. Ecol. Appl. 24, 1289–1296.
Féret, J.B., François, C., Asner, G.P., Gitelson, A.A., Martin, R.E., Bidel, L.P., Ustin, S.L., Marie, G., Jacquemoud, S., 2008. PROSPECT-4 and 5: advances in the leaf optical properties model separating photosynthetic pigments. Remote Sens. Environ. 112, 3030–3043.
Ferreira, M.P., Zortea, M., Zanotta, D.C., Shimabukuro, Y.E., de Souza Filho, C.R., 2016. Mapping tree species in tropical seasonal semi-deciduous forests with hyperspectral and multispectral data. Remote Sens. Environ. 179, 66–78.
Gandolfi, S., Joly, C.A., Rodrigues, R.R., 2007. Permeability-impermeability: canopy trees as biodiversity filters. Sci. Agric. 64, 433–438.
Gardner, T.A., Barlow, J., Chazdon, R., Ewers, R.M., Harvey, C.A., Peres, C.A., Sodhi, N.S., 2009. Prospects for tropical forest biodiversity in a human-modified world. Ecol. Lett. 12, 561–582.
Gastellu-Etchegorry, J.P., Demarez, V., Pinel, V., Zagolski, F., 1996. Modeling radiative transfer in heterogeneous 3-D vegetation canopies. Remote Sens. Environ. 58, 131–156.
Gastellu-Etchegorry, J.-P., et al., 2015. Discrete anisotropic radiative transfer (DART 5) for modeling airborne and satellite spectroradiometer and LIDAR acquisitions of natural and urban landscapes. Remote Sens. 7, 1667–1701.
Gitelson, A.A., Zur, Y., Chivkunova, O.B., Merzlyak, M.N., 2002. Assessing carotenoid content in plant leaves with reflectance spectroscopy. Photochem. Photobiol. 75, 272–281.
Guo, L., Chehata, N., Mallet, C., Boukir, S., 2011. Relevance of airborne lidar and multispectral image data for urban scene classification using random forests. ISPRS J. Photogramm. Remote Sens. 66, 56–66.
Haboudane, D., Miller, J.R., Tremblay, N., Zarco-Tejada, P.J., Dextraze, L., 2002. Integrated narrow-band vegetation indices for prediction of crop chlorophyll content for application to precision agriculture. Remote Sens. Environ. 81, 416–426.
Hernández-Clemente, R., Navarro-Cerrillo, R.M., Zarco-Tejada, P.J., 2012. Carotenoid content estimation in a heterogeneous conifer forest using narrow-band indices and PROSPECT + DART simulations. Remote Sens. Environ. 127, 298–315.
Houborg, R., McCabe, M., Cescatti, A., Gao, F., Schull, M., Gitelson, A., 2015. Joint leaf chlorophyll content and leaf area index retrieval from Landsat data using a regularized model inversion system (REGFLEC). Remote Sens. Environ. 159, 203–221.
Huesca, M., García, M., Roth, K.L., Casas, A., Ustin, S.L., 2016. Canopy structural attributes derived from AVIRIS imaging spectroscopy data in a mixed broadleaf/conifer forest. Remote Sens. Environ. 182, 208–226.
Ito, A., 2011. A historical meta-analysis of global terrestrial net primary productivity: are estimates converging? Glob. Chang. Biol. 17, 3161–3175.
Jacquemoud, S., et al., 2009. PROSPECT+ SAIL models: a review of use for vegetation characterization. Remote Sens. Environ. 113, S56–S66.
Kimes, D.S., Kirchner, J.A., 1982. Radiative transfer model for heterogeneous 3-D scenes. Appl. Opt. 21, 4119–4129.
Laurin, G.V., Chan, J.C.W., Chen, Q., Lindsell, J.A., Coomes, D.A., Guerriero, L., ... Valentini, R., 2014. Biodiversity mapping in a tropical west African forest with airborne hyperspectral data. PLoS One 9, e97910.
Leitão Filho, H.F., 1982. Aspectos taxonômicos das florestas do estado de São Paulo. Silvicultura em São Paulo, São Paulo.
Levizou, E., Drilias, P., Psaras, G.K., Manetas, Y., 2005. Nondestructive assessment of leaf chemistry and physiology through spectral reflectance measurements may be misleading when changes in trichome density co-occur. New Phytol. 165, 463–472.
Liaw, A., Wiener, M., 2002. Classification and regression by randomForest. R News 2, 18–22.
Malenovský, Z., Martin, E., Homolová, L., Gastellu-Etchegorry, J.-P., Zurita-Milla, R., Schaepman, M.E., Pokorný, R., Clevers, J.G.W., Cudlín, P., 2008. Influence of woody elements of a Norway spruce canopy on nadir reflectance simulated by the DART model at very high spatial resolution. Remote Sens. Environ. 112, 1–18.
Malenovský, Z., Homolová, L., Zurita-Milla, R., Lukeš, P., Kaplan, V., Hanuš, Gastellu-Etchegorry, J.-P., Schaepman, M.E., 2013. Retrieval of spruce leaf chlorophyll content from airborne image data using continuum removal and radiative transfer. Remote Sens. Environ. 131, 85–102.
Menze, B.H., Kelm, B.M., Masuch, R., Himmelreich, U., Bachert, P., Petrich, W., Hamprecht, F.A., 2009. A comparison of random forest and its Gini importance with standard chemometric methods for the feature selection and classification of spectral data. BMC Bioinf. 10 (1).
Morellato, L.P.C., 1991. Estudo da fenologia de árvores, arbustos e lianas de uma floresta semidecídua no sudeste do Brasil. Ph.D. Dissertation (Ecology). UNICAMP, Campinas, Brasil.
Morsdorf, F., Kükenbrink, D., Schneider, F.D., Abegg, M., Schaepman, M.E., 2018. Close-range laser scanning in forests: towards physically based semantics across scales. Interface Focus 8 (2), 20170046.
Morton, D.C., Rubio, J., Cook, B.D., Gastellu-Etchegorry, J.P., Longo, M., Choi, H., Hunter, M., Keller, M., 2016. Amazon forest structure generates diurnal and seasonal variability in light utilization. Biogeosciences 13, 2195–2206.
Myneni, R.B., Hoffman, S., Knyazikhin, Y., Privette, J.L., Glassy, J., Tian, Y., ... Lotsch, A., 2002. Global products of vegetation leaf area and fraction absorbed PAR from year one of MODIS data. Remote Sens. Environ. 83 (1), 214–231.
Nave, A.G., 1999. Determinação de unidades ecológicas num fragmento de floresta nativa, com auxílio de sensoriamento remoto. Master dissertation (Forest science). ESALQ/USP, Piracicaba, Brasil.
Pal, M., 2005. Random forest classifier for remote sensing classification. Int. J. Remote Sens. 26, 217–222.
Pan, Y., Birdsey, R.A., Fang, J., Houghton, R., Kauppi, P.E., Kurz, W.A., ... Ciais, P., 2011. A large and persistent carbon sink in the world's forests. Science 333, 988–993.
Poorter, L., Bongers, L., Bongers, F., 2006. Architecture of 54 moist-forest tree species: traits, trade-offs, and functional groups. Ecology 87 (5), 1289–1301.
Price, C., 1994. How unique are spectral signatures? Remote Sens. Environ. 49, 181–186.
Richter, R., Reu, B., Wirth, C., Doktor, D., Vohland, M., 2016. The use of airborne hyperspectral data for tree species classification in a species-rich Central European forest area. Int. J. Appl. Earth Obs. Geoinf. 52, 464–474.
Roberts, D.A., Gardner, M., Church, R., Ustin, S., Scheer, G., Green, R.O., 1998. Mapping chaparral in the Santa Monica Mountains using multiple endmember spectral mixture models. Remote Sens. Environ. 65, 267–279.
Roberts, D.A., Halligan, K.Q., Dennison, P.E., 2007. ViperTools. Retrieved from. http://www.vipertools.org, Accessed date: 17 February 2013.
Schäfer, E., Heiskanen, J., Heikinheimo, V., Pellikka, P., 2016. Mapping tree species diversity of a tropical montane forest by unsupervised clustering of airborne imaging spectroscopy data. Ecol. Indic. 64, 49–58.
Schlerf, M., Atzberger, C., 2006. Inversion of a forest reflectance model to estimate structural canopy variables from hyperspectral remote sensing data. Remote Sens. Environ. 100, 281–294.
Schneider, F.D., Leiterer, R., Morsdorf, F., Gastellu-Etchegorry, J.-P., Lauret, N., Pfeifer, N., Schaepman, M.E., 2014. Simulating imaging spectrometer data: 3D forest modeling based on LiDAR and in situ data. Remote Sens. Environ. 152, 235–250.
Schneider, F.D., Morsdorf, F., Schmid, B., Petchey, O.L., Hueni, A., Schimel, D.S., Schaepman, M.E., 2017. Mapping functional diversity from remotely sensed morphological and physiological forest traits. Nat. Commun. 8, 1441.
Smolander, S., Stenberg, P., 2003. A method to account for shoot scale clumping in coniferous canopy reflectance models. Remote Sens. Environ. 88, 363 − 373.
Theodorsson-Norheim, E., 1986. Kruskal-Wallis test: BASIC computer program to perform nonparametric one-way analysis of variance and multiple comparisons on ranks of several independent samples. Comput. Methods Prog. Biomed. 23 (1), 57–62.
Verhoef, W., Jia, L., Xiao, Q., Su, Z., 2007. Unified optical-thermal four-stream radiative transfer theory for homogeneous vegetation canopies. IEEE Trans. Geosci. Remote Sens. 45, 1808–1822.
Verrelst, J., Camps-Valls, G., Muñoz-Marí, J., Rivera, J.P., Veroustraete, F., Clevers, J.G., Moreno, J., 2015. Optical remote sensing and the retrieval of terrestrial vegetation bio-geophysical properties–a review. ISPRS J. Photogramm. Remote Sens. 108, 273–290.
Wang, Y.P., Houlton, B.Z., 2009. Nitrogen constraints on terrestrial carbon uptake: implications for the global carbon-climate feedback. Geophys. Res. Lett. 36, L24403.
Widlowski, J.L., et al., 2015. The fourth phase of the radiative transfer model intercomparison (RAMI) exercise: actual canopy scenarios and conformity testing. Remote Sens. Environ. 169, 418–437.
Wright, J.S., 2002. Plant diversity in tropical forests: a review of mechanisms of species coexistence. Oecologia 130 (1), 1–14.
Wright, I.J., Reich, P.B., Westoby, M., Ackerly, D.D., Baruch, Z., Bongers, F., et al., 2004. The worldwide leaf economics spectrum. Nature 428, 821−−827.
Xiao, Y., Zhao, W., Zhou, D., Gong, H., 2014. Sensitivity analysis of vegetation reflectance to biochemical and biophysical variables at leaf, canopy, and regional scales. IEEE Trans. Geosci. Remote Sens. 52, 4014–4024.
Yin, T., Gastellu-Etchegorry, J.P., Lauret, N., Grau, E., Rubio, J., 2013. A new approach of direction discretization and oversampling for 3D anisotropic radiative transfer modeling. Remote Sens. Environ. 135, 213–223.
Zarco-Tejada, P.J., Guillén-Climent, M.L., Hernández-Clemente, R., Catalina, A., González, M.R., Martín, P., 2013. Estimating leaf carotenoid content in vineyards using high resolution hyperspectral imagery acquired from an unmanned aerial vehicle (UAV). Agric. For. Meteorol. 171, 281–294.
Zeng, Y., Li, J., Liu, Q., Huete, A.R., Yin, G., Xu, B., ... Mu, X., 2016. A radiative transfer model for heterogeneous agro-forestry scenarios. IEEE Trans. Geosci. Remote Sens. 54, 4613–4628.